In-situ monitoring of epitaxial ferroelectric thin-film growth

Review Article

Author(s):
Sarott, Martin F.; Gradauskaite, Elzbieta; Nordlander, Johanna; Strkalj, Nives; Trassin, Morgan

Publication date:
2021-06-09

Permanent link:
https://doi.org/https://doi.org/10.3929/ethz-b-000479735

Originally published in:
Journal of Physics: Condensed Matter 33(29), https://doi.org/10.1088/1361-648X/abf979

Funding acknowledgement:
- Multifunctional oxide electronics using natural ferroelectric superlattices ()
- Designing oxide electronics with light ()
- In-situ second harmonic generation for emergent electronics in transition-metal oxides ()

To cite this article before publication: Martin F Sarott *et al* 2021 *J. Phys.: Condens. Matter* in press https://doi.org/10.1088/1361-648X/abf979

Topical Review

In-situ monitoring of epitaxial ferroelectric thin-film growth

Martin F. Sarott*, Elzbieta Gradauskaite*, Johanna Nordlander, Nives Strkalj and Morgan Trassin

Department of Materials, ETH Zurich, Vladimir-Prelog-Weg 4, 8093 Zurich

* authors contributed equally to this work

E-mail: morgan.trassin@mat.ethz.ch

Abstract

In ferroelectric thin films, the polarization state and the domain configuration define the macroscopic ferroelectric properties such as the switching dynamics. Engineering of the ferroelectric domain configuration during synthesis is in permanent evolution and can be achieved by a range of approaches, extending from epitaxial strain tuning over electrostatic environment control to the influence of interface atomic termination. Exotic polar states are now designed in the technologically relevant ultrathin regime. The promise of energy-efficient devices based on ultrathin ferroelectric films depends on the ability to create, probe, and manipulate polar states in ever more complex epitaxial architectures. Because most ferroelectric oxides exhibit ferroelectricity during the epitaxial deposition process, the direct access to the polarization emergence and its evolution during the growth process, beyond the realm of existing structural in-situ diagnostic tools, is becoming of paramount importance. We review the recent progress in the field of monitoring polar states with an emphasis on the non-invasive probes allowing investigations of polarization during the thin film growth of ferroelectric oxides. A particular importance is given to optical second harmonic generation in situ. The ability to determine the net polarization and domain configuration of ultrathin films and multilayers during the growth of multilayers brings new insights towards a better understanding of the physics of ultrathin ferroelectrics and further control of ferroelectric-based heterostructures for devices.

Table of contents

1. Introduction

With this review, we aim to give an overview of the recent developments in the advanced characterization during the design of epitaxial thin films of ferroelectric oxides. We begin with a brief motivation in Section 1, emphasizing the potential of polar materials for energy-efficient electronics and discussing the challenges that are faced with the integration of ultrathin ferroelectric films into devices. We also highlight the consequence of the epitaxial growth on the ferroelectric properties. Since most ferroelectric materials are deposited in the ferroelectric phase, the electric polarization can be investigated during the deposition. We then move on to the ferroelectric characterization in Section 2, starting with invasive approaches that involve electrode insertion, sample preparation or probes in contact with the surface. We then continue with non-invasive techniques with a large working distance including X-ray diffraction and optical second harmonic generation. In Section 3, we cover the advances of techniques for in-situ monitoring of the structural and ferroelectric properties of thin films. While electron diffraction allows for monitoring of the growth dynamics, optical second harmonic generation and X-ray diffraction address in situ the targeted functional property in ferroelectrics – the polarization – either directly or indirectly. Section 4 sheds light on the new degrees of freedom that emerge from the ability to directly monitor ferroelectricity during the growth of oxide heterostructures towards the design of robust ferroelectricity in the ultrathin regime. Finally, in Section 5, we give future perspectives going beyond the investigation of ferroelectric materials and passive analysis towards operando investigations. We suggest the possibility to act on the ferroelectric order in situ.

1.1 Energy-efficient electronics using ferroelectrics

Among the ferroic systems, ferroelectrics are attracting the scientific community due to their strong impact on nowadays technologies [1–5]. The energy-efficient electric field drives the remanent electric polarization, which makes ferroelectric materials of interest for memory applications [1,6–9]. Because all ferroelectrics are also intrinsically piezoelectric, the range of applications is further extended towards electromechanical elements and sensors. Within this review, we will focus on the study of ferroelectric polarization, the corresponding surface bound charges, and the domain configuration. The properties and applications related to piezoelectricity have been reviewed in detail elsewhere [2].

Ferroelectric random-access memories (FeRAM) take advantage of the non-volatile polarization of ferroelectric materials. In a metal/ferroelectric/metal capacitor architecture, a voltage pulse is employed to write the polarization state. The readout, however, is destructive: the macroscopic ferroelectric polarization orientation is measured by probing the occurrence of a switching event induced by the application of an electric field. When the polarization reverses, the corresponding surface bound charges invert. This induces a switching current that can be monitored. This destructive readout together with the challenge of scaling ferroelectrics (see Section 1.2) is a limiting factor for the development of FeRAM.

The concept of ferroelectric tunnel junctions (FTJs) emerged in the late 2000's [6,10]. FTJs are the ferroelectric analogs of the tunneling magnetoresistance (TMR) heterostructures. The discovery of magnetoresistance in the late 80's [11,12] revolutionized our society and our way to process and store information electronically. In TMR-based magnetic multilayers, a resistance contrast is achieved by controlling the relative orientation of the magnetization of neighboring layers separated by a tunneling barrier. Because the tunneling process preserves the spin orientation, a high tunneling current is only achieved when the ferromagnetic electrodes exhibit the same magnetization orientation. The first magnetic layer acts as an electron spin polarizer for the tunneling current and the second one as an analyzer. The electron tunneling probability can therefore be efficiently manipulated by controlling one magnetic electrode using spin-polarized currents.

In a FTJ, the tunnel barrier is ferroelectric and the resistance between two metallic electrodes (metal-1,2 in Figure 1(a)), i.e. the electroresistance, depends on the polarization orientation in the barrier. Here, the switching of the resistance is achieved with energy-efficient electric fields in contrast to energy-inefficient spin currents, which are needed in the magnetoresistance architectures [13,14]. The different screening lengths $\delta_{1,2}$ of the metallic electrodes drive an asymmetric tunneling potential across the ferroelectric material. This leads to a polarization-dependent FTJ resistance state [10]. For the metal-1/ferroelectric/metal-2 heterostructure described in Figure 1(a), the high to low resistance states can be controlled by an electric-field.

The electroresistance further provides an alternative to the conventional destructive readout of a ferroelectric state [4,15]. Here, the current tunneling through the thin ferroelectric layer conveys the information about the polarization direction. Furthermore, when the metallic electrodes are ferromagnetically ordered, the electroresistance and the aforementioned magnetoresistance can coexist [3,6]. Such a multiferroic memory combines the ferromagnetic and ferroelectric order parameters in a single device architecture and offers four different resistance states considering parallel and antiparallel configurations of the magnetic electrodes and the two polarization states of the barrier [7,9,16].

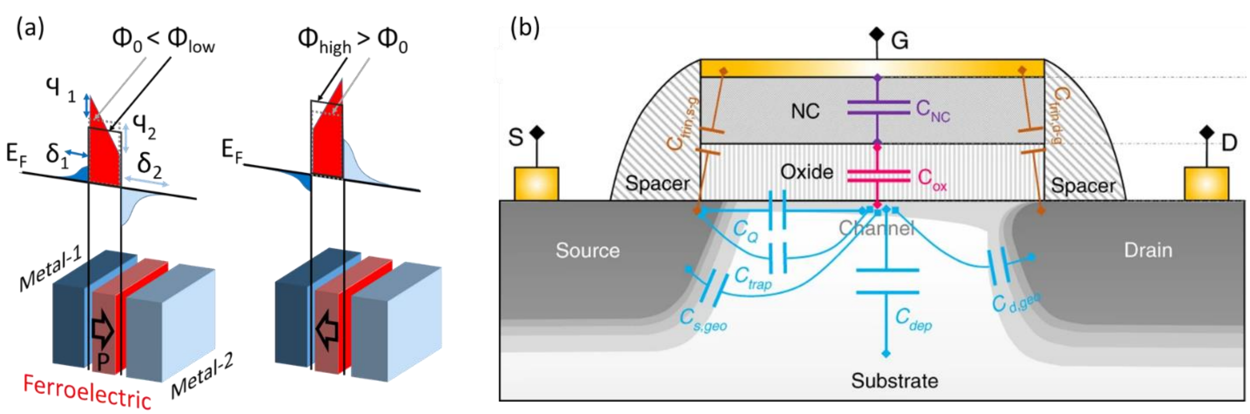

Figure 1. *Ferroelectric tunnel junction and negative-capacitance field-effect transistor. (a) Representation*

of the asymmetric electrostatic potential across a metal-1/ferroelectric/metal-2 stack caused by the different screening of the polarization (P) bound charges due to the unequal screening lengths $\delta_{1/2}$ of the electrodes. The corresponding potential Ч$_i$ adds to the initial square tunneling potential Φ_0 across the barrier and leads to a changed average barrier height Φ_{low} or Φ_{high} depending on the orientation of P. (b) Schematic of a negative-capacitance field-effect transistor with a ferroelectric layer with negative capacitance C_{NC} inside the gate stack. Reprinted from [17].

The existence of remanent surface charges accompanying the ferroelectric polarization further motivates the integration of ferroelectric materials into existing device architectures towards a new generation of transistors [18], i.e. the ferroelectric field effect transistor (Fe-FET) [19,20]. In state-of-the-art FETs, the control of electron flow in the channel between source and drain defines the ON and OFF states. At the gate, a voltage bias is applied in order to induce charge accumulation and activate the channel conductivity. Inserting a ferroelectric material in the gate stack in Fe-FET would allow non-volatile operation of the gate in absence of external bias. Furthermore, in their seminal work, Salahuddin and coworkers [18] suggested that the implementation of a ferroelectric material next to the gate material, could drastically affect the efficiency of current transistor technology beyond the above-mentioned Fe-FET concept. They demonstrated that the insertion of a ferroelectric material next to the insulator material in the gate stack results in an effective negative capacitance (NC) provided by the ferroelectric capacitor, leading to a voltage amplification at the gate channel interface. The first demonstration of this so-called transient negative capacitance [21], see Figure 1(b), triggered an intense interest into NC-FETs [22,23], however, direct technological relevance of NC-FETs remains to be determined [17,24].

The above-mentioned device paradigms rely on robust net polarization with a net charge accumulation at the microscale. While domain and domain wall formation may be relevant for emerging domain-wall-based technologies [25–28], the direct integration of ferroelectrics in device architectures often requires the film to be in a single domain state. In the ultrathin regime, however, the complex interplay of electrostatics and strain poses challenges for obtaining a controlled domain configuration. Furthermore, the suppression of net polarization in the low thickness range hinders the integration of ferroelectrics into oxide electronics. Note that hereafter, we refer to films with thicknesses below 50 unit cells as ultrathin films.

1.2 Ferroelectricity in the ultrathin regime

The domain configuration in thin ferroelectric films determines the net polarization state and the polarization switching dynamics, thereby defining the application relevance [2,5,29]. It is therefore critical to develop an understanding of domain formation and to achieve deterministic control of ferroelectric domains from a design perspective to improve device efficiency. The physics of ferroelectric materials in the technologically relevant ultrathin regime, however, has remained under intense investigation. The spontaneous polarization is accompanied by the accumulation of surface bound charges [29]. This charge accumulation in turn creates a so-called depolarizing field, which is oppositely oriented to the polarization in the film. When the thickness is reduced, the increasing impact of the depolarizing field drives polarization suppression in the films, for instance via the formation of oppositely oriented domains [30–36]. Therefore, control over the charge-screening environment is a key step towards a deterministic domain structure in ferroelectric films. Figure 2(a) displays the wide range polarization states and domain configurations depending on the electrostatic environment. When sufficient screening of bound charge is provided, a single domain configuration with polarization direction out-of-plane can be stabilized. In absence of screening, the polarization suppression is triggered through nanoscale domain formation, rotation of polarization direction to in-plane, or reduction of Curie temperature (T_C). On the one hand the resulting complex physics offers new avenues for the design of polarization states and domain configurations depending on the electrostatic environment. Complex arrays of dipole moments [5] such as flux closure quadrants [37], ferroelectrics vortices [38], polar merons [39], and skyrmions [40] can thus emerge. On the other hand, it renders the synthesis of ferroelectric films with a controlled polarization state challenging, which limits their direct device integration [30].

In the early 2000s, Junquera and Ghosez addressed the efficiency of metals for screening ferroelectric bound charge in a metal/ferroelectric/metal capacitor and discussed the fundamental size limits for ferroelectrics in such capacitor architectures [41]. First principle calculations revealed that in the realistic scenario, the finite screening length at the metal/ferroelectric interface leads to uncompensated interface charges. Therefore, the residual depolarizing field suppresses the ferroelectric behavior in ultrathin capacitors. In the case of $BaTiO_3$ films with $SrRuO_3$ electrodes, the ferroelectric polarization is suppressed below a thickness of 6 unit cells in the capacitor. Surprisingly, even in ferroelectric films with thickness beyond the critical thickness, polarization suppression has been found to occur [36,42–44]. This observation was later experimentally explained with the demonstration of a transient enhancement of the depolarizing field during the growth of the top $SrRuO_3$ electrode that leads to domain formation in $BaTiO_3$-based ultrathin capacitors. Figure 2(b) shows a cross sectional transmission electron microscopy image of a $SrRuO_3/BaTiO_3/SrRuO_3$ capacitor [30]. The nanoscale domains induced by the depolarizing field are visualized in Figure 2(c).

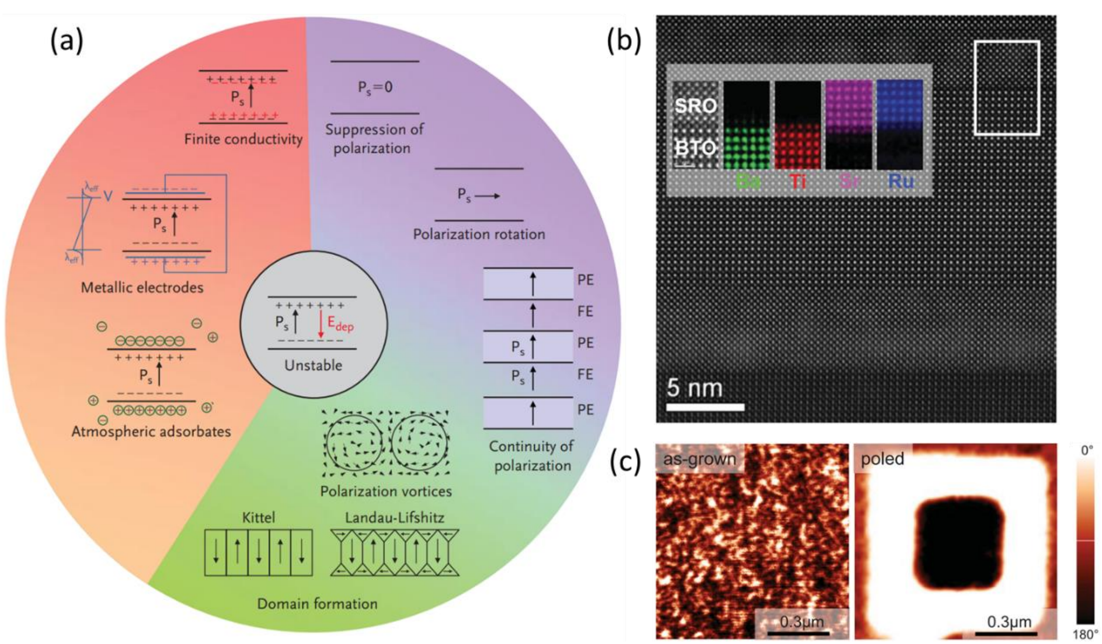

***Figure 2**. (a) Illustration of the impact of the electrostatic environment on the polarization and domain configuration* [29]*. Reproduced with permission (Copyright 2012 Wiley-VCH Verlag GmbH & Co. KGaA). (b) Scanning transmission electron microscopy cross section of a prototypical $SrRuO_3/BaTiO_3/SrRuO_3$ (SRO/BTO/SRO) capacitor with an element specific energy-dispersive X-ray analysis across the top interface in the inset. (c) Piezoresponse force microscopy images showing the $BaTiO_3$ domain splitting caused by the depolarizing field (left). The local electric-field-induced switching (right) confirms the ferroelectric nature of the $BaTiO_3$ thin film. (b,c) Reprinted with permission from* [30]*. Copyright 2019 by the American Physical Society.*

Acting pre- or post-synthesis on the bound charge at either the bottom interface, by introducing metallic buffer electrodes and atomic-scale interface engineering [45–47], or at the top interface, by introducing charge screening environments such as gases [48,49], liquids [50–52], or defects [53], have been so far the preferred approaches in engineering the domain configuration despite their limited potential for industrial implementation. The scientific community only recently started understanding the ferroelectric nature of the films during the deposition process [46,54]. As described in the next section, the exertion of epitaxial strain can significantly increase the ferroelectric transition temperature, such that the domain formation may already take place during the growth process itself.

1.3 Ferroelectricity at the epitaxial growth temperature

Achieving high quality deposition of epitaxial thin films requires a high level of control of the deposition flux and elevated growth temperatures for crystallization (ranging usually between 400°C and 900°C). Physical vapor deposition (PVD) techniques including pulsed laser deposition (PLD), radio-frequency magnetron sputtering, and molecular beam epitaxy (MBE) meet these requirements and have therefore been established as the most prominent techniques for the fabrication of epitaxial thin films. The growth process relies on the material evaporation from a source followed by the transport of the species to a heated substrate, all of which takes place in the controlled environment of a vacuum chamber. For PLD and sputtering, the material source, referred to as target, typically consists of a sintered ceramic pellet of the desired stoichiometry. The target material is ablated by a pulsed UV laser or by bombardment with high-energy ions during PLD and sputtering, respectively. In MBE, the material flux is generated by the evaporation or sublimation of individual chemical elements in effusion cells. In comparison to PLD and sputtering, despite the reduced deposition rate, the single element sources used for the MBE growth process allow for materials engineering at the atomic scale. For further reading on PVD techniques and the epitaxial growth of films, we recommend the following literature on PLD [55–58], sputtering [58], and MBE [58,59]. Note that all these PVD growth processes involve ultra-high vacuum growth chambers with a geometry that is compatible with in-situ investigations. In particular, optical access to the films inside the deposition system is a common feature and a prerequisite for in-situ structural investigations. The techniques for in-situ monitoring of ferroelectricity in epitaxial films, discussed in Sections 3.2 and 3.3, can therefore be implemented in any epitaxial growth processes.

Irrespective of the PVD method used for epitaxial growth, the elevated growth temperatures have direct implications on the stability of the ferroelectric phase during growth. Only a few ferroelectric materials, such as $LiNbO_3$ [60] and $BiFeO_3$ [7,29], exhibit a bulk ferroelectric transition temperature above the growth temperature. Many other ferroelectrics, including $BaTiO_3$ and $PbTiO_3$, have a bulk Curie temperature well below the temperatures that are required for epitaxial growth. However, because of the strong lattice-polarization coupling in ferroelectric materials, epitaxial strain has been found to lead to a giant enhancement of the ferroelectric transition temperature [46,61–63]. Similar to the enhancement of ferroelectricity under hydrostatic pressure [64], the lattice deformation in ferroelectric films which is induced by the lattice mismatch with the substrate or the buffer layer drastically impacts the ferroelectric state of the films [65]. In fact, for most ferroelectric oxides, the Curie temperature is elevated by the exertion of both compressive and tensile strain [62,63,66], to such an extent that even a small lattice mismatch with the substrate can result in the emergence of ferroelectricity during the thin film growth. A T_C above growth temperature constitutes an important requirement for in-situ investigations of ferroelectricity during growth, as covered in Sections 3.2 and 3.3. For instance, ferroelectric $BaTiO_3$ has a bulk Curie temperature of only 120°C, yet epitaxial strain values of less than 2% imposed by common substrates such as $SrTiO_3$ increase the Curie temperature by several hundreds of degrees to temperatures that well exceed the typical growth temperature of 650°C. Figure 3(a) presents the epitaxial-strain-dependent ferroelectric phase diagram of $BaTiO_3$ [62].

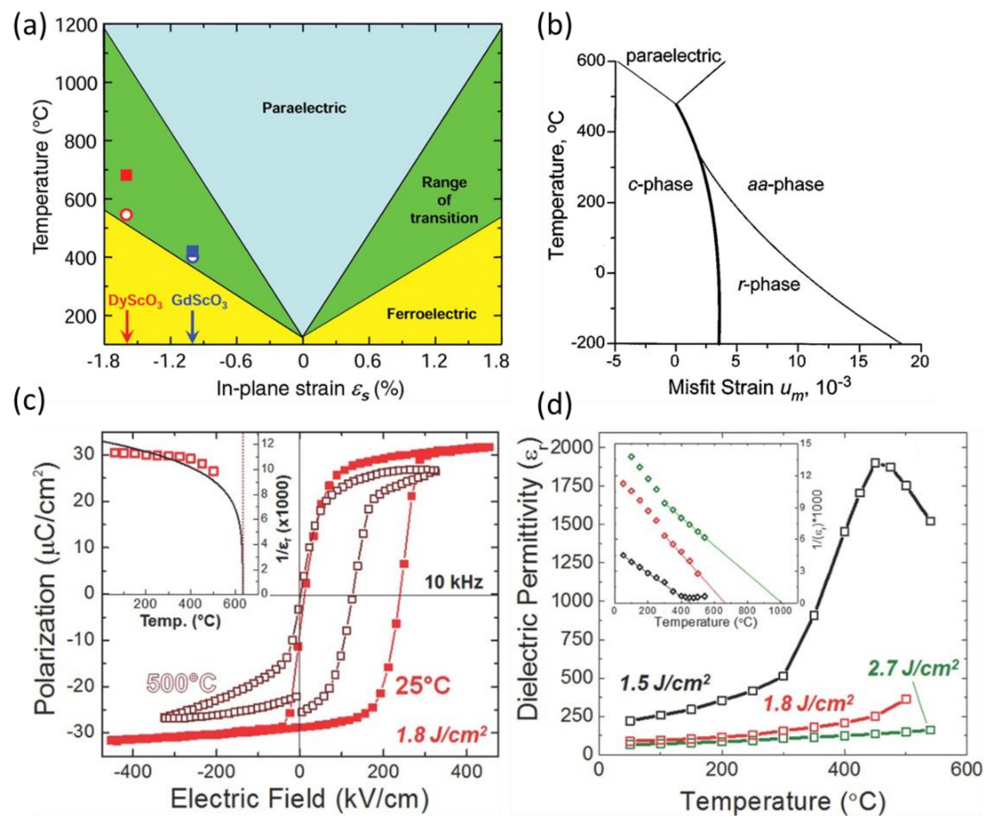

***Figure 3**. Strain-engineering of the ferroelectric transition temperature in epitaxial thin films. The strain-temperature phase diagrams for $BaTiO_3$ (a) and $PbTiO_3$ (b) reveal an increase of the transition temperature for both compressive and tensile in-plane strain. (a) From* [62]*. Reprinted with permission*

from AAAS. (b) Reprinted with permission from [66]*. Copyright 1988 by the American Physical Society. (c,d) The strain-induced alignment of defect dipoles can enhance the polarization and the transition temperature of $BaTiO_3$ on $GdScO_3$. A high laser fluence during PLD growth leads to the incorporation of charged defects that are aligned by the compressive strain. (c,d) From* [67]*. Reproduced with permission (copyright 2014 Wiley-VCH Verlag GmbH & Co. KGaA).*

Similarly, high compressive strain results in an increased ferroelectric transition temperature for $PbTiO_3$ films [66,68], see Figure 3(b). Strain can even induce ferroelectricity in films that are typically paraelectric [69–73]. When grown on tensile-straining $DyScO_3$ substrates, films of the incipient ferroelectric $SrTiO_3$ exhibits ferroelectricity with an in-plane polarization at room temperature [70]. Furthermore, although not ferroelectric in bulk, a strain-induced polarization has been reported in thin films of $CaMnO_3$ [73], $SrMnO_3$ [72], and $KTaO_3$ [71].

In addition to epitaxial strain, defect-dipole ordering during thin-film growth can further enhance the Curie temperature. Damodaran *et al.* [67] have shown that using a high laser fluence during pulsed laser deposition results in an increased density of charged defects during the growth of $BaTiO_3$. The strain-induced alignment of defect dipoles during thin-film growth favors the emergence of polarization, and further increases the spontaneous polarization and ferroelectric transition temperature above the values expected solely from epitaxial strain, as depicted in Figures 3(c) and 3(d). Even though compressive epitaxial strain is still required for the defect-dipole related enhancement, this study revealed a promising route for polarization enhancement that could go beyond the strain-induced enhancement and provide new degrees of freedom robust against strain relaxation effects.

In conclusion, in most cases, the ferroelectric phase is stable at the epitaxial growth temperature and the polarization state is set during the epitaxial growth process. The boundary conditions that define the most energetically favorable ferroelectric domain structure are constantly changing during processing in terms of thickness, electrostatic screening, strain state, and defect density. The thin-film growth conditions are therefore not only control parameters for the crystalline quality, but also for the emergence of ferroelectricity in terms of polarization magnitude and domain configuration. The final response of a ferroelectric layer is the result of the deposition history of the sample.

2. Probing ferroelectricity in epitaxial layers in the ultrathin regime

In Section 1.1, we briefly addressed the technological relevance of ferroelectric thin films. In order to successfully integrate ultrathin layers of ferroelectrics into device architectures, the dominating role of the surface charges and of the depolarizing field on the domain formation needs to be further explored. Let us now discuss the available tools for the investigation of ferroelectricity in thin films in Section 2. This has been the topic of several detailed reviews [5,74–78], we will therefore restrict ourselves to the recent investigations of ultrathin layers, insisting on the most commonly used techniques. We distinguish invasive and non-invasive techniques, the latter ones being compatible with in-situ investigations during the epitaxial deposition, as discussed in Section 3.

2.1 Invasive probes of ferroelectricity

The electric polarization density is defined as the average dipole moment per unit volume. Electric dipoles result from the off-centering of the center of mass of positive and negative charges with respect to each other, mainly because of ionic displacements [75,79,80]. For example, in the prototypical ferroelectric perovskite $BaTiO_3$, ferroelectricity emerges as a consequence of the displacement of the Ti^{4+} ion within the oxygen octahedral cage. The resulting spontaneous polarization creates the accumulation of surface bound charges. The measurement of the ferroelectric hysteresis and its main features, i.e. coercive field, remanent, and saturation polarization commonly quantified in $\mu C/cm^2$, are based on the detection of the bound charge movements, which accompany a polarization reversal. The current corresponding to the movement of bound charges during the ferroelectric switching event is integrated and normalized to obtain the polarization of the specimen. However, such measurements necessitate the insertion of metallic electrodes at both interfaces and further patterning of the ferroelectric film and are therefore intrusive.

Ferroelectric hysteresis and positive-up-negative-down (PUND) characterization - Ideal ferroelectrics should be insulating, however, in reality they often exhibit finite electrical conductivity related to defects [81] or impurities [82]. This additional charge displacement gives rise to a leakage current, which interferes with the electrical hysteresis measurement [83]. If interpreted as bound charge, this leads to measurement artifacts resulting in a cigar-shaped polarization-electric field (P-E) hysteresis loop indicative of lossy dielectrics. The increased amount of scientific literature dealing with artefact-dominated P-E loops motivated J. F. Scott to highlight the distinction between intrinsic and extrinsic contributions in the ferroelectric hysteresis in the now famous article entitled “Ferroelectrics go bananas” [77]. He compared the hysteresis loop obtained from a proper ferroelectric $Ba_2NaNb_5O_{15}$ and the one measured on a dielectric banana skin, see Figure 4(a) and 4(b), respectively. The ferroelectric hysteresis without leakage current has a characteristic shape with concave regions and polarization converging towards saturation polarization at high fields, as measured for a real ferroelectric in Figure 4(b). In order to exclude the contribution from leakage currents, the PUND measurement technique [75,84–86] is commonly used. It consists of a sequence of voltage pulses with repeated polarity. Subtracting the currents measured during two successive pulses with the same polarity allows to extract the currents which are not related to the ferroelectric switching event. An alternative method to account for leakage current has been proposed that relies on dynamic leakage current compensation [87].

Interfacial effects at electrodes may still affect hysteresis measurements even if a perfect ferroelectric film is assumed. Since ferroelectrics are wide band-gap semiconductors, these interfaces are typically modelled as Schottky contacts [88]. Different Schottky barriers at the two interfaces of a ferroelectric layer are the reason for commonly observed asymmetries between the positive and negative branches of the current-voltage (I-V) characteristics [88] and further measurement artefacts [89]. The barrier height can be minimized by improving the interface quality and selecting electrode materials with better screening properties [90]. The electrode material is also a decisive factor for ferroelectric performance, most notably the ferroelectric fatigue [91–93], which corresponds to a gradual decrease of the ferroelectric polarization upon electrical cycling. In the context of epitaxial thin films, metallic oxides, such as $SrRuO_3$, $La_{1-x}Sr_xMnO_3$ (LSMO), $LaNiO_3$, $In_2O_3 : SnO_2$ (ITO), $YBa_2Cu_3O_{7-x}$ (YBCO), and $Ce_xCa_{1-x}MnO_3$ (CCMO) are commonly selected as bottom electrodes because of their excellent lattice matching with most perovskite-based ferroelectric materials [94]. They also lead to better endurance of the ferroelectric switching [95]. Top electrodes are generally based on single-element metals and conventionally deposited post-growth to simplify lithographic post-processing. In particular, Pt, Cu, Au, Ag, or Pd are established materials for top electrodes [96].

Piezoresponse force microscopy (PFM) - PFM belongs to the family of scanning probe techniques, where a conducting probe is brought in direct contact with the ferroelectric film surface. PFM is commonly used to study ferroelectricity locally by detecting a contrast in the piezoresponse from spontaneously formed or electrically induced ferroelectric domains. PFM also offers some more elaborate measurements, including the identification of critical parameters of domain nucleation [97] and dynamics [98], as well as quantitative maps of local switching characteristics [99]. Additionally, it offers the capability of imaging intricate polar structures, such as ferroelectric vortex domains [100] or nanoscale bubble domains [101], as shown in Figure 4(c) and 4(d). For more literature dealing with the recent progress in PFM, we recommend the following reviews [74,102]. An important limitation of surface-sensitive PFM is its probing depth, resulting in the inaccessibility of buried domains in ferroelectric-based heterostructures within thick layers or once the ferroelectric layer is capped. A new variant of PFM involves a highly-controlled milling process during the tip scanning in order to resolve the domain configuration in three dimensions [103]. This approach, called tomographic PFM, overcomes the limitations mentioned above at the price of being destructive. It is worth mentioning that even though PFM is a very accessible technique that is relatively easy to interpret, one has to be aware of potential artifacts that arise mostly from electrostatics [104,105].

Scanning transmission electron microscopy (STEM) - The transmission electron microscopy techniques took a leap forward with the introduction of aberration-corrected magnetic lenses [106,107] as well as the ever-ongoing progress in sample preparation using focused ion beam (FIB) milling [108–110]. These improvements enabled the mapping of atomic displacements at a sub-angstrom scale [111] and the local determination of the polarization direction and magnitude within each unit cell in a thin sample lamella. This microscopic approach drastically advanced the understanding of nanoscale polar arrays [112] and unveiled previously unresolvable features such as Néel-type ferroelectric domain walls [113,114], ferroelectric closure domains [37,115,116], polar vortices [38], and polar skyrmions [40], as shown in Figure 4(e)-(g).

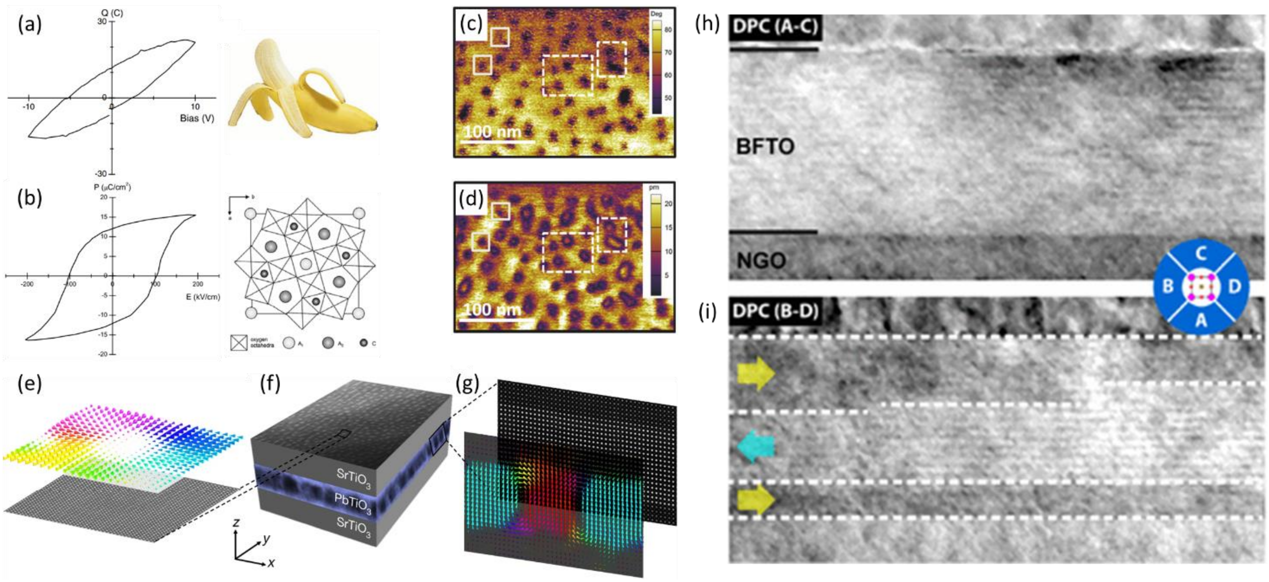

Figure 4. *(a) Typical charge vs. voltage loop obtained for a dissipative dielectric, such as a banana skin. (b) Characteristic P-E hysteresis loop for the ferroelectric material $Ba_2NaNb_5O_{15}$. (a,b) From* [77]*. Reprinted with permission from IOP Publishing Copyright (2007). Piezoresponse force microscopy phase (c) and amplitude (d) images of nanoscale bubble domains in a $PbZr_{0.2}Ti_{0.8}O_3$ / $SrTiO_3$ (2 u.c.) / $PbZr_{0.2}Ti_{0.8}O_3$ heterostructure. (c,d) From* [101]*. Reproduced with permission (copyright 2017 Wiley-VCH Verlag GmbH & Co. KGaA). (e-g) Observation of a polar skyrmion structure in a $[(PbTiO_3)_{16}/(SrTiO_3)_{16}]_8$ superlattice. The displacement vector map (e) based on the atomically resolved plane-view HAADF-STEM image of a single skyrmion bubble shows the hedgehog-like skyrmion structure. The sketch of the superlattice in (f) is overlaid with the planar-view dark-field TEM image providing a top view of the superlattice. (g) The displacement vector map (front) based on the atomically resolved cross-sectional HAADF-STEM image (back) reveals a cylindrical domain with anti-parallel (up–down) polarization. (e-g) Reprinted by permission from Macmillan Publishers Ltd: Nature* [40]*. Copyright 2019. (h,i) Differential-phase contrast STEM images of a thin films of the in-plane ferroelectric $Bi_5FeTi_3O_{15}$ on $NdGaO_3$. By using a segmented detector, it is possible to selectively image out-of-plane (h) and in-plane (i) electric field components inside the sample. (h,i) Reprinted with permission from* [117]*. Copyright © 2019 American Chemical Society.*

STEM analysis is compatible with temperature dependent investigations. For instance, the order-disorder ferroelectric phase transition of improper geometrically-driven ferroelectrics has been imaged in situ in real space [118]. For dedicated reviews on STEM capacity, we recommend the following works [119,120]. A recently developed STEM mode called differential phase contrast (DPC) imaging [117,121] is based on the deflection of the electron beam due to internal electric fields in the sample. When applied to ferroelectrics it opens alternative ways for directly visualizing ferroelectric domains. Figure 4(h) and 4(i) show the DPC contrast corresponding to ferroelectric domains in a layered Aurivillius ferroelectric material with in-plane polarization [117]. Because of the uniaxial nature of these ferroelectric films, the domain contrast only appears when the imaging sensitivity is set along the unique polarization axis.

The characterization techniques, described in this section, provide quantitative information on the ferroelectric property. They, however, remain intrusive or destructive and challenging in the ultrathin regime. The insertion of electrodes for the voltage application for either the determination of the ferroelectric hysteresis or the piezoresponse characterization is incompatible with polarization monitoring when the ferroelectricity emerges during the epitaxial growth. We will now go through alternative non-invasive approaches giving access to ferroelectricity.

2.2 Non-invasive probes of ferroelectricity

Among the noninvasive probes, two techniques stand out as particularly useful for studying ferroelectricity in thin films. First, X-ray diffraction experiments access the structural distortions that accompany the emergence of a ferroelectric phase. Such studies therefore constitute an indirect probe of ferroelectricity and further enable the detection of periodicities induced by the formation of ordered domains [122]. Second, the nonlinear optical process – optical second harmonic generation (SHG) [76,123,124] – is sensitive to inversion symmetry breaking and is therefore an ideal diagnostic tool for probing ferroelectricity remotely.

X-ray diffraction (XRD) - XRD is a powerful technique to characterize the crystal structure of materials, which can be used to infer information about the ferroelectric polarization and domain configuration. Seminal experiments dealing with thin films of the tetragonal ferroelectric model system $PbTiO_3$ demonstrated the power of XRD-based analysis in investigating ferroelectricity in the ultrathin regime [125]. The ferroelectric polarization is indirectly accessed by measuring the lattice expansion along the polarization direction, i.e. the change of the long *c*-axis lattice parameter in the tetragonal $PbTiO_3$ unit cell. Lichtensteiger et al. [125] investigated the evolution of tetragonality (ratio of the out-of-plane polar *c*-axis and the in-plane *a*-axis lattice parameters, denoted *c/a*) as a function of decreasing thickness in epitaxial $PbTiO_3$ films on metallic Nb-doped $SrTiO_3$ substrates. A decrease in the *c*-axis parameter was observed for thicknesses below 20 nm and attributed to the depolarizing field, see Figure 5(a). Because of the large probing depth of XRD, studies of the polarization state in ferroelectric-based capacitors [126] and ferroelectric/dielectric superlattices [38–40] then followed.

In non-uniaxial ferroelectric systems, where the polarization can point in several directions, XRD-based reciprocal space mapping (RSM) can be used to identify the presence of different domain variants with distinct structural distortions [127]. A prototypical system for such studies is rhombohedral ferroelectric $BiFeO_3$ [7,128]. Eight possible polarization directions are allowed along the crystallographic $\langle 111 \rangle$ directions of the pseudo-cubic unit cell [7]. The monoclinic distortions associated with the polarization directions are traceable by XRD, as shown in Figure 5(b). The lattice elongation along the polar axis gives rise to a periodic variation in the projection of the unit cell onto the diffraction plane in the direction of the polarization. The presence of ferroelectric variants thus correlates with the appearance of peak splitting around the pseudo-cubic $BiFeO_3$ Bragg reflections. XRD experiments have been used to support domain engineering in $BiFeO_3$ towards the deterministic control of domain variants using anisotropic in-plane epitaxial strain from the substrate [129] or surface vicinality [130]. XRD also gives insights into the domain distribution in terms of the volume of in-plane and out-of-plane domains (*a*-domains and *c*-domains) in tetragonal ferroelectric $PbTiO_3$ [53,125], $Pb(Zr,Ti)O_3$ (PZT) [114,131] and $BaTiO_3$ [132] thin films.

In addition to the correlation between the polarization amplitude and the lattice deformation, ferroelectric domains often arrange in periodic structures that can be accessed by XRD experiments. In particular, 180° domains exhibit an architecture characterized by an average domain width of the stripe-like configuration (Figure 5(c)). For the case of a purely out-of-plane polarized system, the 180° domain formation expresses itself in reciprocal space as in-plane diffuse scattering around the characteristic Bragg peaks [126,133,134]. However, the reduced sample volume of thin films used for XRD experiments limits the determination of the domain configuration in the ultrathin regime. Therefore, the vast majority of XRD experiments deal with ferroelectric superlattices, in which ferroelectric thin films of a few unit cells in thickness are stacked in periodic structures. Ferroelectric/dielectric, more specifically $PbTiO_3/SrTiO_3$, superlattices emerged as the model system for such analysis. A typical domain ordering in the $PbTiO_3/SrTiO_3$ superlattice is depicted in Figure 5(c). The reciprocal space mapping of the structures exhibits the structural periodicity of the superlattice in the Q_z direction while the domain periodicity results in diffuse scattering in the Q_{xy} direction shown in Figure 5(d). The small lattice parameter mismatch between $PbTiO_3$ and $SrTiO_3$ allows for total thicknesses of several hundred nanometers without the relaxation of strain.

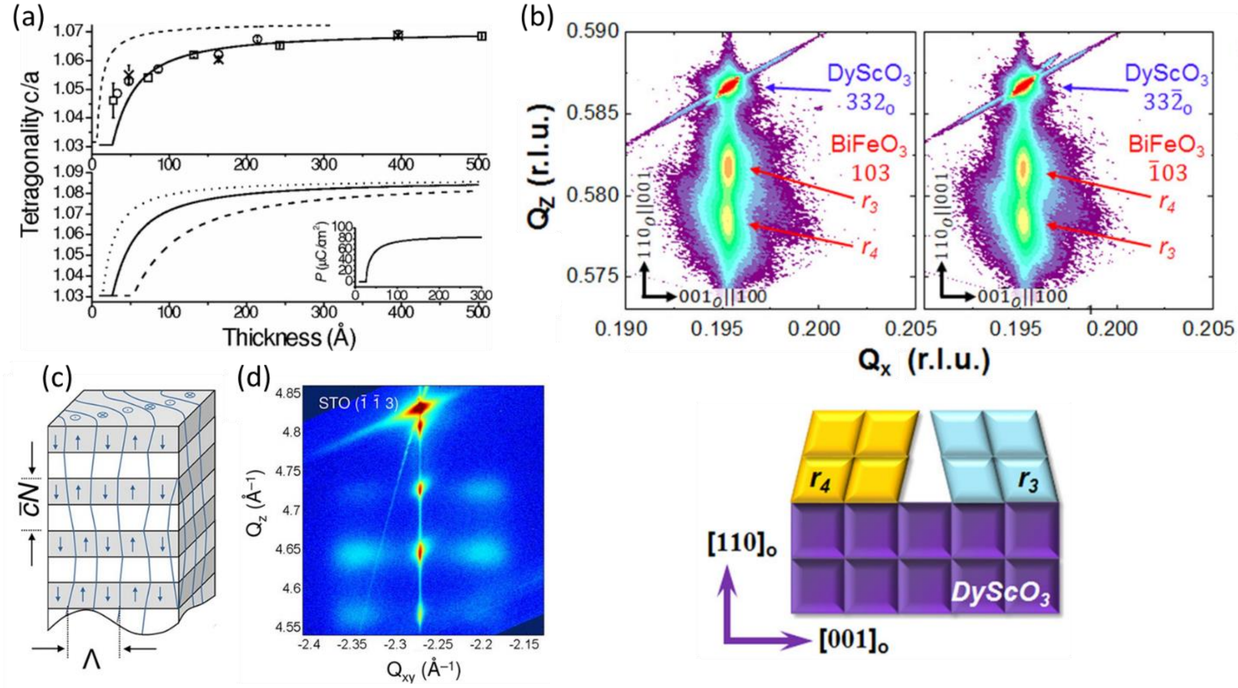

Figure 5*. (a) Thickness dependence of tetragonality for ferroelectric $PbTiO_3$ films. The top panel compares experimental data (circles, squares, crosses) a with phenomenological theory prediction (dashed line) and a model Hamiltonian (solid line). The lower panel shows the results obtained from a set of model Hamiltonian calculations. Reprinted with permission from* [125]*. Copyright 2005 by the American Physical Society. (b) Reciprocal space maps of a 50 nm $BiFeO_3$ film grown on $DyScO_3$. The two domain variants r_3 and r_4 (bottom schematic) manifest as a peak splitting of the $BiFeO_3$ Bragg peaks. From* [127]*. Reprinted with permission from AIP Publishing. Copyright 2014. (c) Representation of the typically encountered periodicities in ferroelectric/dielectric superlattices. (d) Reciprocal space map of an $(PbTiO_3)_{10}/(SrTiO_3)_{10}$ superlattice around the $SrTiO_3$ $(\bar{1}\bar{1}3)$ peak exhibiting superlattice peaks along Q_z and diffuse in-plane scattering due to the domain periodicity. (c,d) Reprinted with permission from* [133]*. Copyright © 2012, American Chemical Society.*

Finally, resonant X-ray diffraction experiments that allow determination of the polarization orientation in ferroelectric thin films are under development [135]. Friedel's law, stating that structure factors of pair reflections hkl and $\bar{h}\bar{k}\bar{l}$ are equivalent, is broken in the case of resonant scattering. Polarization orientation as well as polarization reversal events are therefore traceable using resonant experiments [136].

Optical second harmonic generation - Laser-optical techniques provide a complementary platform to diffraction methods for the non-invasive and electrode-free study of ferroelectric materials. Amongst them, the most prominent technique is optical second harmonic generation (SHG) as the lowest-order nonlinear optical process [76,123,124]. Optical SHG describes the frequency doubling of light in matter, where an incident light field $E_{j,k}$ at frequency ω induces a polarization P_i at frequency 2ω, acting as the source of the generated frequency-doubled light. In the leading-order electric-dipole approximation, this light-matter interaction is parametrized by the second-order susceptibility tensor $\chi^{(2)}$ and can be macroscopically expressed by the following equation:

$$P_i(2\omega) = \varepsilon_0 \chi_{ijk}^{(2)} E_j(\omega) E_k(\omega)$$

Non-zero tensor components χ_{ijk} are only present for systems that violate spatial inversion symmetry, where the indices i, j, and k indicate the directions of the oscillating fields with respect to the crystal axes. On the one hand, this condition is fulfilled for the case of materials with a non-centrosymmetric point group. On the other hand, the SHG light emission is also possible at surfaces or interfaces of centrosymmetric materials [137]. Such macroscopic discontinuities locally cause a lowering of symmetry, the removal of an inversion center and thus the emergence of non-zero χ_{ijk} tensor components. It should be emphasized that before the establishment of SHG as a powerful probe for ferroic states [76,123,124,138–143], SHG used to be devoted to the study of surface and interface states in centrosymmetric materials [137]. Additionally, the surface electronic states of a wide range of material classes, including metals [144,145], semiconductors [146,147], and insulators [148,149] can be accessed with SHG. Here, we highlight efforts dealing with remote access to surface morphologies and ferroelectric domain states in thin films.

SHG has become an indispensable probe for ferroelectric materials, in which the polar distortion breaks inversion symmetry leading to non-zero χ_{ijk} tensor components. By setting the polarization of the incident probe beam (j,k) and the detected SHG light (i), it becomes feasible to access individual $\chi^{(2)}$ tensor components and thus analyze the polar distortion along certain crystallographic directions. SHG, especially when used in combination with other techniques such as PFM or STEM imaging, provides new insights into ferroelectric domain [68,123,138,142,150] and domain-wall configurations [114,151]. For instance, in ferroelectric $BiFeO_3$ thin films, SHG was employed to monitor the impact of an anisotropic in-plane strain on the formation of 71° domain stripe patterns. Figure 6(a) shows the evolution of the domain configuration imaged by PFM and the corresponding angular dependence of SHG light polarization when in-plane substrate strain anisotropy is exerted by a 5 nm thick LSMO-buffered $DyScO_3$ substrate. The in-plane projection of the spontaneous polarization for the strain-induced 71° domain stripe pattern adds up to an average net in-plane polarization perpendicular to the domain walls. As a direct consequence, the SHG signal in transmission, obtained for varying angles of incident light polarization, exhibits a two-fold symmetry where the dominant lobe is oriented along the polar axis. In the absence of in-plane epitaxial strain, i.e. when a strain-relaxed 10 nm thick LSMO buffer in introduced, a random domain configuration hosting four degenerate ferroelectric domain states and zero net in-plane polarization is established, see Figure 6(b). Here, the polarization-dependent SHG signal becomes sample-orientation independent and mainly originates from non-ferroelectric surface contributions [142].

Since SHG is a direct probe of the material symmetry, in some specific cases, it can provide a unique perspective on the domain investigation of ferroelectric thin films that could not be revealed using solely conventional ferroelectric probing techniques. We will now present some of the insights uniquely provided using the SHG probe.

In the case of the technologically relevant tetragonal ferroelectrics, SHG is only sensitive to a polar distortion projected onto a plane perpendicular to the *k*-vector of the incident light. For instance, in $BaTiO_3$ or PZT, the polarization of *c*-domains cannot be probed in normal incidence. In this configuration, SHG remains, however, able to detect in-plane oriented *a*-domains [68,114]. Because SHG does not necessitate the presence of electrodes and is further compatible with remote investigations, it has emerged as an efficient tool to probe domain populations in ferroelectric thin films [30,132,152], even once inserted into device architectures [46,114,132,152].

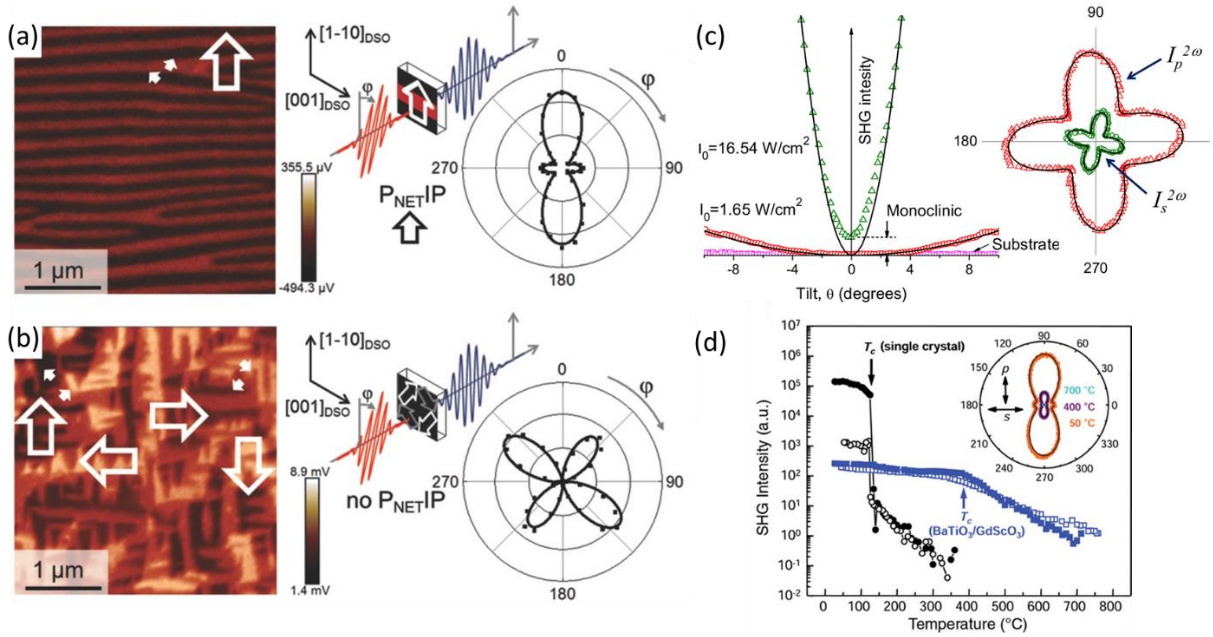

Figure 6. *PFM (left) and SHG (right) signatures of polarization in $BiFeO_3$ thin films under anisotropic in-plane epitaxial strain. The in-plane polarization of the stripe domains (small arrows) adds up to a net in-plane polarization (open arrow) and results in a two-fold symmetry of the SHG signal (b) Corresponding PFM and SHG data in the absence of substrate strain anisotropy. (a,b) From* [142]. *Reproduced with permission (copyright 2015 Wiley-VCH Verlag GmbH & Co. KGaA). (c) SHG tilt scan (left) on a tetragonal $BiFeO_3$ film for two different power densities. The residual signal at zero tilt angle corresponds to the contribution of a monoclinic distortion. On the right, the SHG anisotropy is shown for the two power densities at zero tilt. From* [141]. *Reprinted with permission from AIP Publishing. Copyright 2010. (d) Temperature-dependent SHG measurements on bulk (black) and epitaxially strained $BaTiO_3$ (blue) samples. From* [62]. *Reprinted with permission from AAAS.*

In addition to the sensitivity to a ferroelectric polarization, SHG is also a suitable tool to investigate subtle changes in the crystallographic structure [141,142]. For instance, the non-zero SHG signal appearing in normal incidence for a pure tetragonal $BiFeO_3$ film is correlated to monoclinic distortions, as shown in Figure 6(c).

Another powerful aspect of SHG-based analysis lies in its suitability to monitor ferroic phase transitions [30,62,68]. Whereas electrical measurements often lack reliability at elevated temperatures due to increasing dielectric losses, SHG offers a viable alternative to identify critical temperatures even under applied fields and in harsh environments. In the seminal work by Choi *et al.* [62], SHG was used to quantify the increase of the ferroelectric Curie temperature in epitaxially-strained ferroelectric $BaTiO_3$ films. The SHG signal revealed an increase of T_c of more than 200°C compared to the bulk value, see Figure 6(d).

We emphasize that SHG experiments on ferroelectric thin films require special attention in comparison to experiments on bulk materials due to the reduced domain sizes and the presence of a substrate [123]. Because of the limited optical resolution, SHG requires a net polarization [123]. For non-centrosymmetric substrate materials, a non-zero SHG signal can interfere with the signal from the film and obscure the data analysis. Furthermore, the surface SHG signal can greatly contribute to the total response and even dominate it for a significantly reduced volume of the film. When measuring in transmission, absorption and birefringence effects of the substrate at both the fundamental and the SHG wavelength can hamper the signal detection [76].

3. Probing ferroelectricity during epitaxial growth

As described in Section 1.3, epitaxial strain imposed by single crystalline substrates can favor polar displacements, resulting in an enhancement of the ferroelectric transition temperature. Therefore, as mentioned earlier, most ferroelectric materials grow epitaxially in the ferroelectric phase and ferroelectricity can be investigated already during the deposition, in situ. How tunable is polarization right when it emerges during the deposition? Which new device paradigms can be designed based on the insights into polarization and domain configuration during the deposition? In-situ diagnostics bring answers to these questions and promise to have great impact on, but also beyond, the condensed-matter and functional-materials communities [153].

We start this section describing in-situ monitoring with the most widespread technique: reflection high-energy electron diffraction (RHEED). We also cover emerging in-situ characterization tools, which are becoming essential for precise growth of oxide thin films and led to a major advancement and design of new states of matter, atomic interface engineering, and to the understanding of complex growth processes [154]. The provided insights into the thickness, strain state, surface structure, and chemical composition are complementary to the study of ferroelectricity. These tools remain, however, insensitive to the functionality – the polarization - that is aimed for when growing ferroelectric materials. Seminal studies dealing with XRD in situ [122] marked a new era of investigating ferroelectric materials during the growth. We therefore start in-situ investigations on polar states with diffraction-based experiments. We finally emphasize an emerging approach that gives direct access to the polarization in thin films, namely optical SHG in situ [46].

3.1 In-situ structural monitoring tools for epitaxial growth

The ferroelectric order in thin films exhibits a complex thickness dependence because of the correlation of the electric polarization with the lattice strain and electrostatic boundary conditions. The control over the crystalline quality, orientation and thickness of the films with high accuracy is a prerequisite towards further investigations of the thin film functionality in situ. Let us therefore first go through the existing tools allowing structural monitoring during thin-film synthesis. An essential characteristic of all the techniques described below is their long working distance, compatible with most PVD techniques used for the growth of epitaxial thin films involving extreme conditions with elevated temperatures and high oxygen pressures.

Reflection high-energy electron diffraction (RHEED) - Electron diffraction techniques have been used to monitor growth processes in situ since the 1950s due to the large scattering cross section and forward scattering nature of high-energy electrons when compared to X-rays [155]. RHEED investigations are based on the analysis of reflected and diffracted electrons directed in grazing incidence on the substrate. In the often-desired two-dimensional layer-by-layer growth mode, periodic roughness variations related to changing island step densities result in oscillations of the integrated intensity of the specular reflection in the RHEED pattern. Following these oscillations therefore enables a direct access to the thickness of the film. In addition, monitoring the diffraction pattern of the growing surface makes it possible to determine the film morphology [156] (two-dimensional vs. three-dimensional surface), the strain state [157], and allows the identification of surface reconstructions [158].

A surge of interest in RHEED can be related to the development of molecular beam epitaxy (MBE) in the 1970s [159]. The AlGaAs/GaAs heterostructure is an exemplary system [155,159–162], whose growth by MBE has been facilitated by the use of RHEED. Not only it is used to monitor the deposition rate, but also to identify different surface reconstructions that are crucial in determining the incorporation of species in the growth front and to optimize growth conditions for the semiconductor industry [163]. In addition to semiconductors, RHEED monitoring substantially contributed to the advancement in the deposition of oxide thin films. It allows atomic surface coverage monitoring during oxide MBE and facilitates the timed deposition of individual atomic species. Recent work revealed the consequence of such a control at the atomic scale towards the design of heterostructures with unconventional properties [164]. Furthermore, the direct access to the oxide surface can lead to new degrees of freedom and to the creation of artificial layered materials. For instance, the deposition of synthetic Ruddlesden-Popper homologues [165], using non-stoichiometric RHEED-assisted MBE processes has been demonstrated, as shown in Figure 7(a).

In the 1990s, the development of the differential pumping system allowed RHEED monitoring of growth processes to take place at high oxygen pressures. This triggered an improved control of oxide thin-film growth by pulsed laser deposition (PLD) [166] and radio frequency sputtering [167]. The combination of RHEED and a layer-by-layer growth mode [168] is of particular interest since it allows thickness control with a precision of (sub-)unit cell for the design of increasingly complex oxide superlattices. RHEED analysis is especially important for the growth of perovskite ABO_3-type ferroelectric films in the ultrathin regime, because the polarization direction (upwards-, or downwards-oriented) and domain structure can be controlled by selecting an appropriate surface termination of the buffer layer [46,169]. This is rationalized by changes in growth kinetics [169], the electric potential across the interface [45], atomic plane sequencing [170], or even changes in metallicity [171]. It has been shown that RHEED can capture precisely when the surface termination converts from BO_2 to AO atomic planes during PLD growth [172,173]. Such termination switching can also be achieved artificially by RHEED-assisted deposition of exactly one monolayer of a corresponding oxide [174,175]. Beyond the perovskite oxide growth, RHEED-based investigations dealing with materials crystallizing in more complex unit cells are emerging. Thin films of Aurivillius phase, whose unit cells comprise alternating layers of a variable number of perovskite-octahedra planes interleaved between fluorite-like $[Bi_2O_2]^{2+}$ layers along the *c*-axis, are gaining interest due to their exceptional ferroelectric properties resilient to depolarizing field-related effects in the ultrathin regime. Despite the complexity of the unit cell, the layer-by-layer growth mode in the system can be achieved during PLD growth [176], see Figure 7(b). Similarly, sub-unit cell precision was revealed when using RHEED monitoring during the growth of multifunctional $YMnO_3$ [177] and magnetoelectric $GaFeO_3$ [178,179] thin films, see Figures 7(c) and 7(d), respectively.

In-situ Auger electron spectroscopy (AES) - Chemical composition of the surface layer during thin-film growth can be tracked with in-situ AES. Conventionally, AES is carried out in an ultra-high vacuum chamber and provides access to the chemical composition of surfaces due to the elemental specificity of the Auger electron energy spectrum after excitation [180,181]. Measuring AES in an oxide growth chamber in situ is challenging due to the high oxygen pressures required for oxide epitaxy. Yet, recently oscillations in elemental Auger spectra during the layer-by-layer growth of complex oxide heterostructures were reported for the growth of $CaTiO_3$/$LaMnO_3$ superlattices [182], see Figure 8(a). This approach offers full chemical information of the surface layer, complementary to the structural diagnostic provided by RHEED. We highlight the importance of such information in the context of ferroelectric materials where surface chemical composition and termination govern the final polarization [45–47,183].

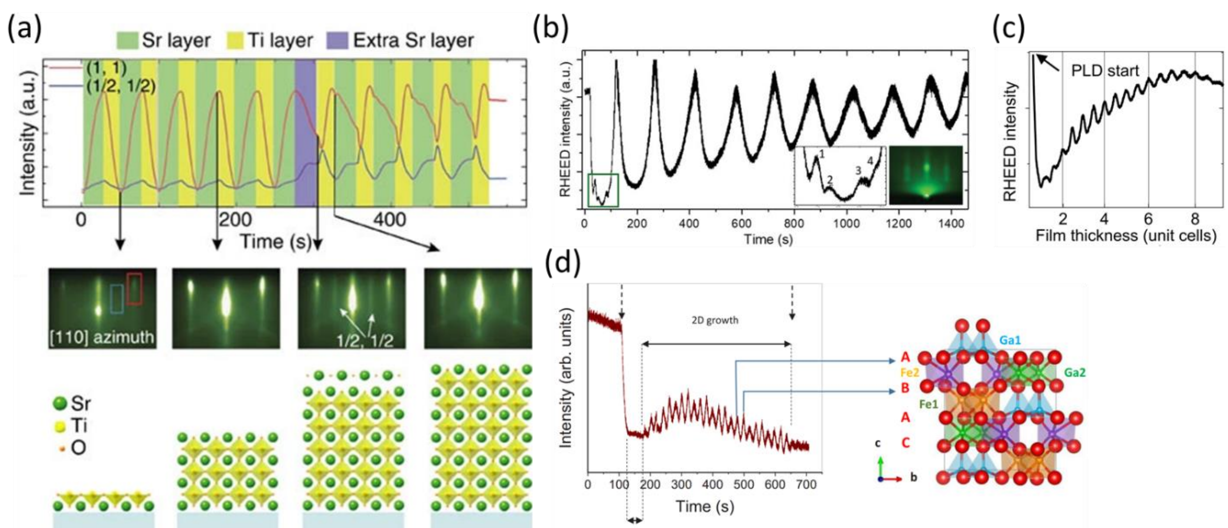

Figure 7. *(a) RHEED intensity oscillations during the deliberate non-stoichiometric MBE growth of $Sr_{n+1}Ti_nO_{n+1}$ Ruddlesden–Popper phase for integer (red) and half-integer (blue) diffraction streaks (top panel) with the corresponding RHEED patterns (middle panel). The insertion of an extra SrO layer leads to a strong increase of the half-integer peak intensity. Cartoon models taken at different stages of the*

growth are displayed in the bottom panel. From [165]*. (b-d) RHEED intensity oscillations for a set of thin films of complex oxides, including (b) ferroelectric Aurivillius $Bi_5FeTi_3O_{15}$, (c) multiferroic hexagonal $YMnO_3$, and (d) multiferroic $Ga_{0.6}Fe_{1.4}O_3$. Each RHEED oscillation corresponds to the growth of half a unit cell (b and c) or a quarter of a unit cell (d). (b) From* [176]*. Reproduced with permission (copyright 2020 Wiley-VCH Verlag GmbH & Co. KGaA). (c) Reprinted with permission from* [177]*. Copyright 2020 by the American Physical Society. (d) Reprinted with permission from* [178]*. Copyright 2019 by the American Physical Society.*

In-situ spectroscopic ellipsometry (SE) – Ellipsometry measurements rely on the detection of light polarization changes upon reflection from a sample and allow the determination of film thickness and optical constants. Typically, SE-data are collected for a set of incoming light polarizations and wavelengths. Being an optical technique with a long working distance, spectroscopic ellipsometry can be conveniently integrated into any deposition process and operated at any growth pressure [184]. Most of the reported literature on in-situ SE deal with diagnostics during atomic layer deposition (ALD) [185]. Standard ALD is performed in cycles and in-situ SE is performed after each corresponding thickness increment. Growth processes of nanolaminate films can be tracked with submonolayer precision, as shown in Figure 8(b) for Er_2O_3-Al_2O_3 film. The amplitude ratio and the phase angle oscillate with each half-cycle due to chemisorption or removal of precursor surface groups, while an overall increase (decrease) in signal is related to a thickness change that can be calculated from a Cauchy model. In-situ SE can provide a variety of optical film properties and can capture changes in surface groups, nucleation behavior, and crystalline phases [185]. The experimental data are easy to collect, but the data analysis requires extensive modelling and fitting [186]. Ferroelectric materials have so far been investigated with ex-situ SE exclusively, involving measurements of dielectric function [187,188], optical conductivity [188], band gap [188–195], ferroelectric phase transition [193,196,197], critical thickness for strain relaxation [198], refractive index, and extinction coefficient [188–192,194,199]. A recent report of in-situ SE monitoring during the growth of Ruddlesden-Popper phase shows that deposition of each epitaxial layer can be detected with submonolayer precision [200], confirming the potential of this technique for monitoring the growth of polar thin films in the near future.

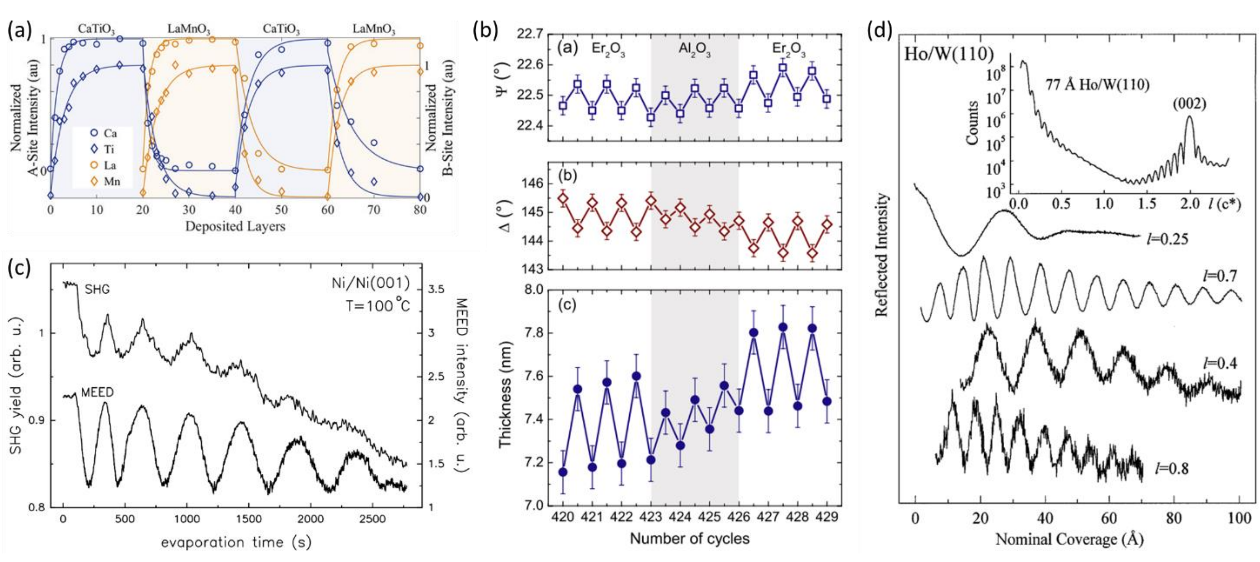

Figure 8. *(a) In-situ AES used to monitor the surface layer during the growth of a $CaTiO_3$/$LaMnO_3$ superlattice. The graph shows the normalized (to the oxygen signal) elemental Auger spectra, collected in situ between depositions of known thickness. Reprinted with permission from* [182]. *Copyright 2019 by the American Vacuum Society. (b) In-situ SE monitoring during ALD growth of Er_2O_3 and Al_2O_3. The amplitude ratio (top panel) and phase angle (middle panel) at a photon energy of 3.0 eV is measured after precursor dosing (half-integer points) and after the O_2 plasma step (full-integer points). The change in thickness (bottom panel) is calculated with a Cauchy model. From* [185]. *Reprinted with permission from IOP Publishing. Copyright 2009. (c) SHG oscillations during the homoepitaxial growth of Ni using electron beam evaporation. The oscillation period of the SHG measurement matches oscillations obtained from electron diffraction. From* [201]. *Reprinted with permission from Springer Nature. Copyright 1969. (d) XRR oscillations during the deposition of Ho on W (110) at room temperature for four different scattering vectors $q = lc^*$ (c^*- reciprocal lattice parameter). The inset displays the diffracted intensity along [00l] for an annealed film. Reprinted with permission from* [202]. *Copyright 1997 by the American Physical Society.*

Optical SHG of surfaces - As described in Section 2.2, SHG is the simplest nonlinear optical process. Surface SHG has been rapidly implemented into the growth chamber environment as a deposition-monitoring tool [201,203–206]. For materials crystallizing in a centrosymmetric point group, the bulk response of the material is not the leading source of the SHG signal, leaving the surface as the dominating SHG contributor. This SHG surface contribution has been employed since the late 80's to monitor surface reconstructions during layer-by-layer growth of GaAs [204]. In combination with in-situ RHEED, providing structural surface information, surface SHG brought new insight in the growth mechanism of semiconductors. While in this case, SHG probes surface electronic states, RHEED probes the long-range order of newly formed surfaces. Furthermore, SHG has been shown to be highly sensitive to surface morphologies with altered electronic states such as step terraces [144]. During the Frank-Van der Merwe layer-by-layer growth mode, ad-atoms diffuse on the surface and form islands that coalesce until completion of a full monolayer coverage. This corresponds to a periodic variation of the step terrace density and as a consequence, in analogy to RHEED monitoring, surface SHG intensity oscillations during layer-by-layer growth can be used for thickness determination. Figure 8(c) shows the in-situ surface SHG signature during layer-by-layer growth of a metallic layer in accordance with oscillations obtained from medium-energy electron diffraction (MEED) [201]. Thus, surface SHG analysis can be complementary to ferroelectric SHG investigations, discussed in the Section 2.2.

X-ray growth oscillations - In the last 30 years, the emergence of intense and well-collimated synchrotron-radiation X-ray sources led to the use of XRD for the investigation of thin films with reduced volume. A well-established ex-situ method for determining the thickness of thin films is X-ray reflectivity (XRR) under grazing incidence. XRR thickness measurements are based on internal reflections within the sample layers leading to differences in beam path for out-going X-rays and corresponding interference patterns. The resulting destructive or constructive beam interferences results in oscillations in the angle-dependent total intensity, which can then be used to extract the thicknesses of the individual layers. Analogous measurements can be conducted during the growth in situ. Here, however, the incidence angle is fixed, and the interference corresponds to reflections from successively deposited monolayers. In particular, the so-called anti-Bragg positions are highly sensitive to changes in thickness [122]. From the period and shape of these oscillations as a function of film thickness, additional information on the growth mode as well as on the influence of various growth conditions can be obtained. For instance, the layer-by-layer growth mode leads to a well-defined and periodic coverage and results in periodic oscillations. Similarly to real-time monitoring using RHEED, the X-ray reflection intensity oscillations provide the information at a single monolayer scale. The first report on in-situ monitoring of growth modes using X-ray reflectivity [207] demonstrated oscillating X-ray reflections during the layer-by-layer homoepitaxy of the model system Ge(111) with perfect matching to RHEED oscillations. While early reports on in-situ XRR have been restricted to homoepitaxial films, it has been also implemented in heteroepitaxy, for instance, for the growth of Ho on W(110) [202], as shown in Figure 8(d).

More recently, monitoring the growth of complex oxide thin-films has been reported for layers of $SrTiO_3$ [208], $La_{1-x}Sr_xMnO_3$ [209] as well as for and $BaTiO_3/SrTiO_3$ superlattices [210]. For further reading, we recommend a detailed review dealing with growth monitoring using XRD [211]. Because XRD experiments also provide access to lattice parameter information, in the next section we will cover the use of XRD to monitor polar distortions in situ.

3.2 Probing ferroelectricity in situ using X-ray diffraction

Among the above mentioned in-situ structural diagnostic tools for epitaxial thin-films deposition, RHEED is by far the most widespread because of its ease of use and real-time information allowing thickness control with unit-cell precision. No information dealing with the functionality, here ferroelectricity, is however available. RHEED lacks sensitivity to the polar distortion, accumulation of surface bound charge accompanying the onset of polarization, as well as to the phase transition through the ferroelectric phase.

Because of the strong lattice-polarization coupling in ferroelectrics, monitoring the distortion of the unit cell brings information on the emergence of the polar axis and hence indirectly the emergence of polarization during the epitaxial deposition. The seminal work dealing with the in-situ XRD characterization of ferroelectricity revealed that the epitaxial strain-enhanced Curie temperature (see Section 1.3) could be determined during in-situ heating of $PbTiO_3$ thin films [61]. The drop of tetragonality by passing into the paraelectric phase unambiguously identifies the Curie temperature. Most importantly, additional periodicity originating from the ordering of ferroelectric domains revealed the unprecedented capacity offered by in-situ XRD. For thin films grown directly on an insulating $SrTiO_3$ substrate, domain formation induced by the depolarizing field was monitored in situ in $PbTiO_3$ [61]. The thickness-dependent appearance of satellite peaks corresponds to the periodic domain formation and indicates the onset of ferroelectricity from the deposition of the third unit cell, as shown in Figure 9(a). This work demonstrated non-invasive access to functionality in the ultrathin regime. For more details, we recommend a review by the pioneers in the field [122]. Here, we highlight the most recent advances in the XRD-based probe of polarization states in thin films in situ.

Two-dimensional reciprocal space mapping (RSM) in situ allows monitoring of the changes of the crystalline structure related to domain formation, as well as the formation of structural defects such as dislocations. In ferroelectric $Ba_{0.5}Sr_{0.5}TiO_3$ films grown on MgO, the strain state and the structural signature of domain formation has been investigated in situ during the growth. Bauer et al. [212] followed the structural distortion of the tensile-strained $Ba_{0.5}Sr_{0.5}TiO_3$ films and the effect of the epitaxial strain relaxation could be visualized. Furthermore, a second crystalline phase could be identified with the appearance of a peak splitting and linked to the formation of ferroelectric domains, as shown in Figure 9(b).

The newest technological developments in the field of in-situ XRD investigations involve a scanning technique that uses the entire available intensity on an area detector to provide the desired information in less time than it takes to deposit a single unit cell of material [210]. During the growth, the out-of-plane and in-plane lattice parameters, the artificially created superlattice repeat periodicity, and the spacing of ferroelectric domains can all be obtained by performing RSM around appropriate Bragg reflections. Bein et al. [210] took advantage of the capacity of scanning RSMs to probe the behavior of ultrathin ferroelectric layers in superlattice heterostructures, as illustrated in Figure 9(c). For the first time, the impact of the electrostatic boundary conditions on the polarization and domain configuration of the ferroelectric thin films were addressed in real time, during the growth of a $BaTiO_3/SrTiO_3$ superlattice. In particular, they demonstrated that the $BaTiO_3$ ferroelectric material can polarize the $SrTiO_3$ dielectric layer grown on its surface up to a dielectric thickness, at which energy minimization favors the formation of domains in the ferroelectric material.

Thus, in-situ XRD contributes to the improvement of the understanding of materials growth in the ferroelectric phase because of its unique ability to quantitatively measure changes in lattice parameters and monitor structural periodicities. We discussed above the formation of domains during synthesis, the impact of strain relaxation on domain formation, and the role of electrostatics [213]. Let us now address another non-invasive probe, which characterizes ferroelectricity through symmetry breaking and which is compatible with the extreme environment of the epitaxial growth: In-situ optical SHG.

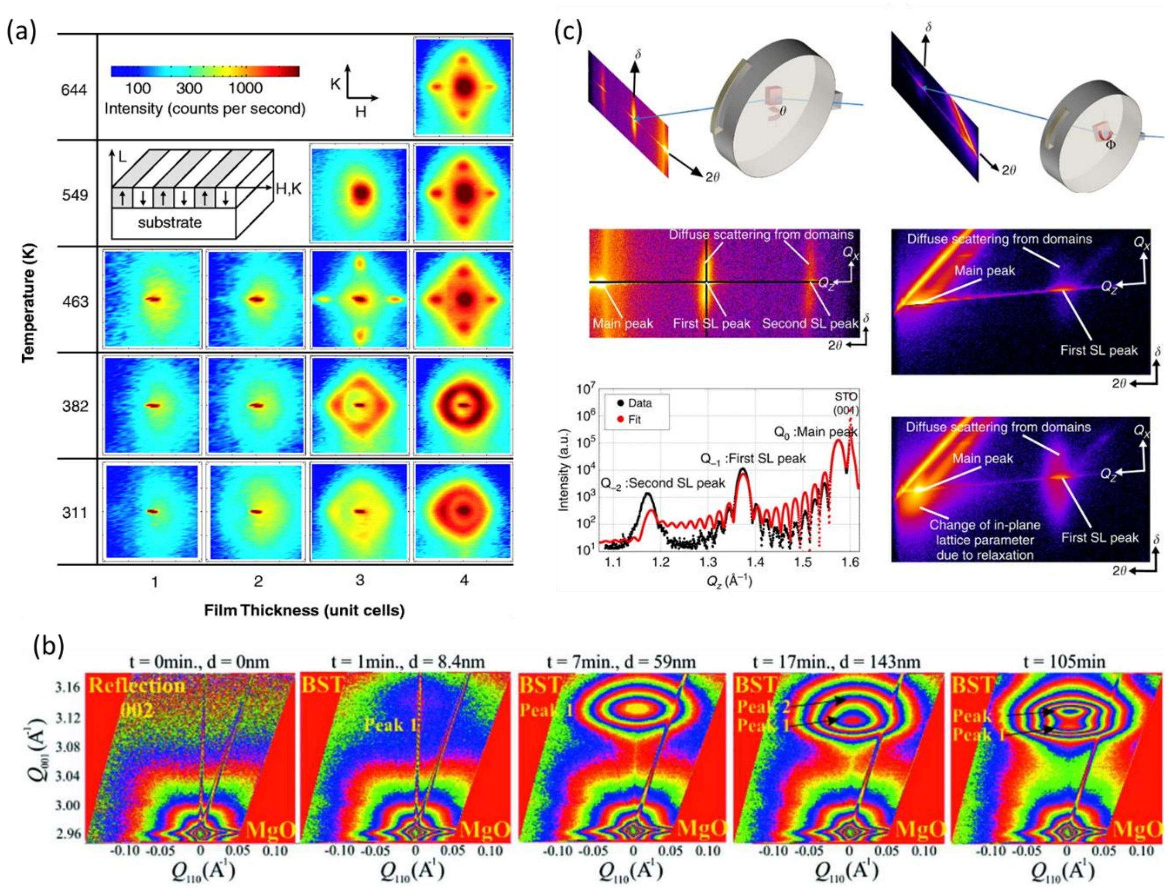

***Figure 9**. (a) In-plane reciprocal space maps around the $PbTiO_3$ (303) Bragg peak measured in situ for different temperatures and thicknesses of $PbTiO_3$ on $SrTiO_3$. The appearance of satellite peaks denotes the onset of ferroelectric ordering and reflects the periodicity in the domain configuration. From* [61]*. Reprinted with permission from AAAS. (b) Sequence of reciprocal space maps acquired during the PLD growth of $Ba_{0.5}Sr_{0.5}TiO_3$ on MgO around the (002) Bragg peak. The appearance of a single peak after 1 min is followed by a peak splitting at 17 min, which is assigned to the formation of ferroelectric domains. Reprinted from* [212]*. (c) Schematic of the experimental setup (top panels) using an area detector to enable the acquisition of (00l) and (10l) reciprocal space maps. In $BaTiO_3/SrTiO_3$ superlattices, the ultrafast data acquisition allows the tracing of superlattice peaks and diffuse scattering from domain formation after completion of 10 bilayers (middle panels) and 30 bilayers (bottom right panel). Reprinted from* [210].

3.3 Probing ferroelectricity-induced symmetry breaking using nonlinear optics

The use of nonlinear optics as a non-invasive diagnostic tool to study materials properties during synthesis was first proposed in the 1980s [204,206], as discussed in Section 3.1. In particular, optical SHG, sensitive to symmetry breaking at the surface, appeared as a complementary tool to RHEED.

In 1998, the first in-situ SHG experiments on ferroic systems were performed to monitor the thickness-dependent magnetic properties of Co [205] and Ni [201] films on Cu(001) with subsequent efforts dedicated to magnetic multilayers [214]. Jähnke *et al.* [201] managed to identify the critical thickness for in-plane magnetic ordering with the appearance of an asymmetry in the SHG signal induced by the magnetization. In addition, Jin and coworkers [205] observed SHG oscillations with a one monolayer periodicity in the magnetic asymmetry, which they assigned to periodically changing magnetic properties of Co during growth. For Ni films on Cu(001), in addition to the critical thickness for in-plane magnetic ordering, in-situ SHG enabled the direct observation of the transition to an out-of-plane magnetization at higher film thicknesses.

A bit less than 20 years later, Rubano et al. [215] proposed SHG imaging as an oxide growth diagnostic technique to obtain spatially-resolved information. Their proof of concept ex-situ study demonstrates the capability of SHG imaging to detect structural heterogeneities with diffraction-limited resolution. However, the implementation of SHG imaging into a growth chamber had not been realized. In 2017, in-situ SHG (ISHG) was implemented into a PLD growth chamber for the first time, as depicted in Figure 10(a) [46], where both the incident light source and the detection setup can be placed outside the growth chamber on account of the sufficiently long SHG working distance. In ISHG, the inversion symmetry breaking resulting in the emission of second harmonic light is dominated by the non-centrosymmetry of the ferroelectric material.

In a proof of concept experiment, involving ferroelectric multilayers, De Luca et al. demonstrated for the first time the in-situ SHG monitoring of polarization emergence during the growth of ultrathin ferroelectric films [46]. In contrast to XRD-based studies, where additional periodicity due to domain splitting is generally beneficial, SHG directly probes the polarization with a yield that is maximized for single domain states [123,138]. This is because SHG light waves emitted from domains with polarization pointing in opposite directions are out-of-phase and therefore interfere destructively. Hence, no ISHG signal can emerge from a 180˚ domain-split ferroelectric film. Used in combination with RHEED, the ISHG yield is obtained with unit cell thickness accuracy and allows accessing information on the ferroelectric order parameter in real time. The onset of an ISHG signal during the growth of $BiFeO_3$ on $SrRuO_3$-buffered $DyScO_3$ and $BaTiO_3$ on $SrRuO_3$-buffered $SrTiO_3$ unambiguously reveals the critical thickness for ferroelectricity [46]. Furthermore, because the probed volume exceeds the total thickness of the ferroelectric single layers, the relative polarization orientation of each ferroelectric constituent in a multilayer or superlattice architecture can be determined. Destructive interference reveals an antiparallel configuration of the ferroelectric layers, as shown in Figure 10(b). In contrast, when all ferroelectric layers exhibit identical polarization orientations, the signal repeatedly increases. The ISHG technique therefore established itself as a powerful tool to qualitatively investigate polarization direction in the ultrathin regime and the effect of interfacial atomic termination. ISHG can be used to monitor in situ the polarization of proper ferroelectric systems such $BaTiO_3$ [30,46], $BiFeO_3$ [46], PZT [47], $PbTiO_3$ [47,68] and improper ferroelectric systems, such as the geometrically-driven ferroelectric hexagonal $YMnO_3$ [118].

Taking advantage of the capacity to directly access the functional property simultaneously with the epitaxial growth, a direct visualization of the domain-formation dynamics in ferroelectric thin films has been shown [68]. The growth of ferroelectric $PbTiO_3$ films was monitored with ISHG to uncover the role of thickness and strain-state in the formation of *a*- and *c*-domains, respectively. The exclusive presence of *c*-domains in $PbTiO_3$ films grown on (001)-oriented $SrTiO_3$ with a 5 nm $SrRuO_3$ bottom electrode leads to the continuous rise of the ISHG signal, shown in Figure 10(c). However, epitaxial tensile strain imposed by (110)-oriented $DyScO_3$ substrate drives a partial conversion of *c*-domains into *a*-domains past a threshold thickness, manifesting as a drop of the ISHG signal yield. The inferred domain states of the two $PbTiO_3$ films were corroborated by PFM and RSM, confirming the sensitivity of the ISHG technique. Most importantly, because this information is acquired in situ, the authors could directly act on the domain formation and shift the *c*-to-*a*-domain conversion to the early stage of the growth, providing a new platform for domain configuration control.

The ISHG intensity is proportional to the square of polarization, it is therefore possible to estimate the polarization enhancement due to epitaxial strain. Figure 10(d) shows the ISHG for $BaTiO_3$ films with a $SrRuO_3$ electrode grown on several substrates. The ISHG yield increase qualitatively confirms how the compressive strain induces a polarization enhancement in $BaTiO_3$ films [30]. By performing in-situ annealing post-growth, as shown in Figure 10(e), or by growing the films at increasing deposition temperature [68], it is further possible to determine the strain-dependent T_c of ferroelectric films using ISHG.

Looking at the functional property directly, in situ and in real time, brings a new capacity to the epitaxial growth of thin-film oxides. Beyond mere monitoring and repeatability assurance, such a capability reveals new degrees of freedom – previously considered inaccessible – that we address in the next section.

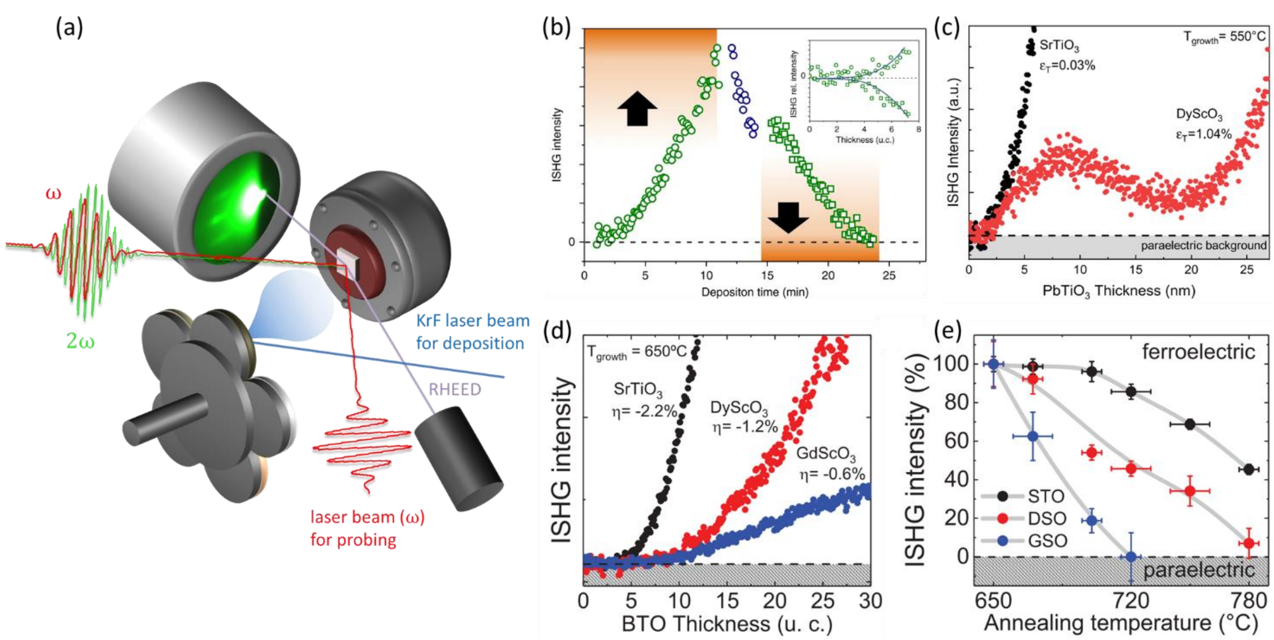

Figure 10. *(a) Schematic of the ISHG experimental setup in a PLD growth chamber with RHEED capability. (b) ISHG measurement during the growth of two $BiFeO_3$ layers with opposite polarization. The SHG signal from the first layer (P up) destructively interferes with the signal from the second layer (P down). Both layers show the same critical thickness (inset). (a,b) Reprinted from* [46]. *(c) ISHG profile during the growth of $PbTiO_3$ on $SrTiO_3$ (black) and $DyScO_3$ (red). The single domain state on $SrTiO_3$ results in a*

continuous signal rise, whereas on $DyScO_3$ a partial c-to-a domain conversion manifests as an ISHG drop. From [68]*. Reprinted with permission from AIP Publishing. Copyright 2020. (d,e) Strain-dependent polarization enhancement in $BaTiO_3$ thin films. An increase in compressive strain leads to an increase in polarization that is reflected in the ISHG yield during growth (d) and a higher Curie temperature as obtained from temperature dependent ISHG measurements (e). (d,e) Reprinted with permission from* [30]*. Copyright 2019 by the American Physical Society.*

4. The benefits of probing ferroelectricity in situ

Most in-situ XRD and SHG studies reported thus far, provide qualitative information on the polarization direction or domain formation during thin-film synthesis. However, quantitative information can equally be extracted. For instance, the ferroelectric transition temperature or the thickness at which the polarization emerges or reaches the bulk value can be quantified with ISHG. Diffraction-based approaches can further quantitatively access thickness- and temperature-dependent lattice parameters and domain periodicities. Quantitative measurements of the ferroelectric polarization in situ are, however, considerably more difficult. Such measurements have not been reported so far, since they require either direct access to switching currents, ex-situ reference measurements [216], or modelling [213], in which the growth conditions are emulated. The qualitative information alone provided by in-situ SHG and XRD have shown their potential to advance the understanding of ferroelectricity in the ultrathin regime and still hold tremendous promise for further explorations.

In particular, in-situ XRD and SHG can reveal important dynamics of the polarization during the deposition process [30,47,68,217]. The electrostatic environment evolves during growth and the surface chemistry changes. We can investigate how the domain configuration gets drastically altered by the device integration under electrostatic changes. The in-situ diagnostic tools described in Section 3.1 contributed to the advancement of the understanding of growth mechanisms and to the optimization of growth processes in general. Similarly, the direct access to the ferroelectric functionality in situ brings new insights into the transient effects and the physics involved in the emergence of ferroelectric domains and to the impact of the growth process on the functionality of the thin films. Let us now highlight recent advances in the field and show how in-situ diagnostics of polarization dynamics during the epitaxial deposition reveals new routes for robust polarization states in the ultrathin regime.

4.1 Electrostatics during epitaxial growth and device integration

As a consequence of the prevailing ferroelectricity at growth temperature, the final polarization of the films drastically depends on the charge screening environment not only during the epitaxial growth but also during the following integration steps into the multilayer architecture. The deposition of capping layers or electrodes on the polar surface becomes a critical factor. Since any deposition starts by the first unit cell coverage, the thickness dependence of the charge screening efficiency or conductivity of the deposited metallic electrode will influence the final polarization state of the ferroelectric films [30,32].

The ferroelectric polarization of $BaTiO_3$ thin films was tracked in situ with ISHG during the integration of the ferroelectric layer in $SrRuO_3$ electrodes [30]. At the end of the $BaTiO_3$ film growth, the constant ISHG signal indicates the good charge screening efficiency of the oxygen rich growth atmosphere [48,49,218,219] and the stable single domain state of the film. An abrupt drop of the net polarization was triggered with the first deposited unit cells of the top $SrRuO_3$ electrode. The first unit cells of $SrRuO_3$ that are poorly conducting isolate the $BaTiO_3$ film from the charge screening growth atmosphere. Figure 11(a) shows the ISHG signal suppression that accompanies the top electrode deposition in the $SrRuO_3$/$BaTiO_3$/$SrRuO_3$ capacitor. Because of the thickness-dependent metallic behavior of the ultrathin $SrRuO_3$ layer, a transient enhancement of the depolarizing field induces a complete polarization suppression. This polarization suppression was identified to be mediated through domain formation. It can be circumvented by performing the top electrode deposition above the Curie temperature of $BaTiO_3$ or by performing a post-growth annealing into the paraelectric phase. In the latter case, the polarization re-emerges during cooling in the charge screening environment of the sufficiently thick top electrode. Interestingly, the ISHG-based real-time access to the domain formation in situ leads to an additional degree of freedom towards controlled domain nucleation induced by the depolarizing field. Interrupting the capping deposition for a given SHG signal intensity, leads to a deterministic domain population in the capped ferroelectric layer.

4.2 Surfaces chemistry and contributions to the polarization states

Monitoring the polarization directly during the thin-film growth further allows the identification of the impact of the deposition process, growth atmosphere, and surface reconstruction on the final polarization. In the ultrathin regime of out-of-plane polarized films, the electrostatic environment sets the net polarization [30,32,35,133]. During the growth, however, in contrast to the influence of the bottom interface, i.e. buffer or substrate, the influence of top interface is not well defined in the evolving growth front.

Engineering ferroelectric domain configuration currently relies on either control of the top or the bottom interface contribution. The polarization direction can be controlled with adequate metallic buffer insertion [30,32] or atomic scale interface engineering [45]. From the top surface, gas [48,49] or liquid [50–52,220] interactions will affect the polarization configuration. The combination of both bottom and top interface contributions sets the final polarization of the films [47,221].

The in-situ approach brings a unique opportunity to independently access each interface contribution. In a pioneering ISHG investigation [47], two different polarization regimes during the epitaxial PLD process of ferroelectric $PbTiO_3$ thin films with a 15 unit cell thick LSMO bottom electrode were identified. During the growth, the charge screening at the bottom interface sets the polarization. It can be deterministically tuned using atomic termination of the buffer and by controlling the interfacial charged planes. In contrast, the influence of the top interface is not well defined because of the long timescale of polarization reconstruction in comparison to the timescale of the growth process. In this transient regime, a single interface therefore influences the polarization direction in the ferroelectric layer. At the growth interruption, a second polarization regime emerges as the top interface settles and contributes to the final polarization. In the case of A-site volatile ferroelectrics, this top interface contribution is dominated by a surface cationic off-stoichiometry, which results in a positively charged surface layer. The distinct access to top and bottom interface contributions brings new insight to the understanding of the final polarization configuration. By manipulating the atomic termination at the bottom interface, the authors could identify cooperative and competitive top and bottom interface contributions. The competitive interface configuration results in a suppression of the ISHG and polarization after completion of the film, see Figure 11(b). In contrast, when both top and bottom interface contributions favor the same polarization direction, a robust single domain configuration could be stabilized in the ultrathin $PbTiO_3$ films. The corresponding giant increase in ISHG yield is shown in Figure 11(c). This polarization is robust against extreme electrostatic environments that usually induce nanoscale domain formation. The STEM dipole map in Figure 11(d) shows that the cooperative interface configuration prevents the domain formation and favors a net polarization despite the capping of the $PbTiO_3$ layer by a $SrTiO_3$ dielectric layer.

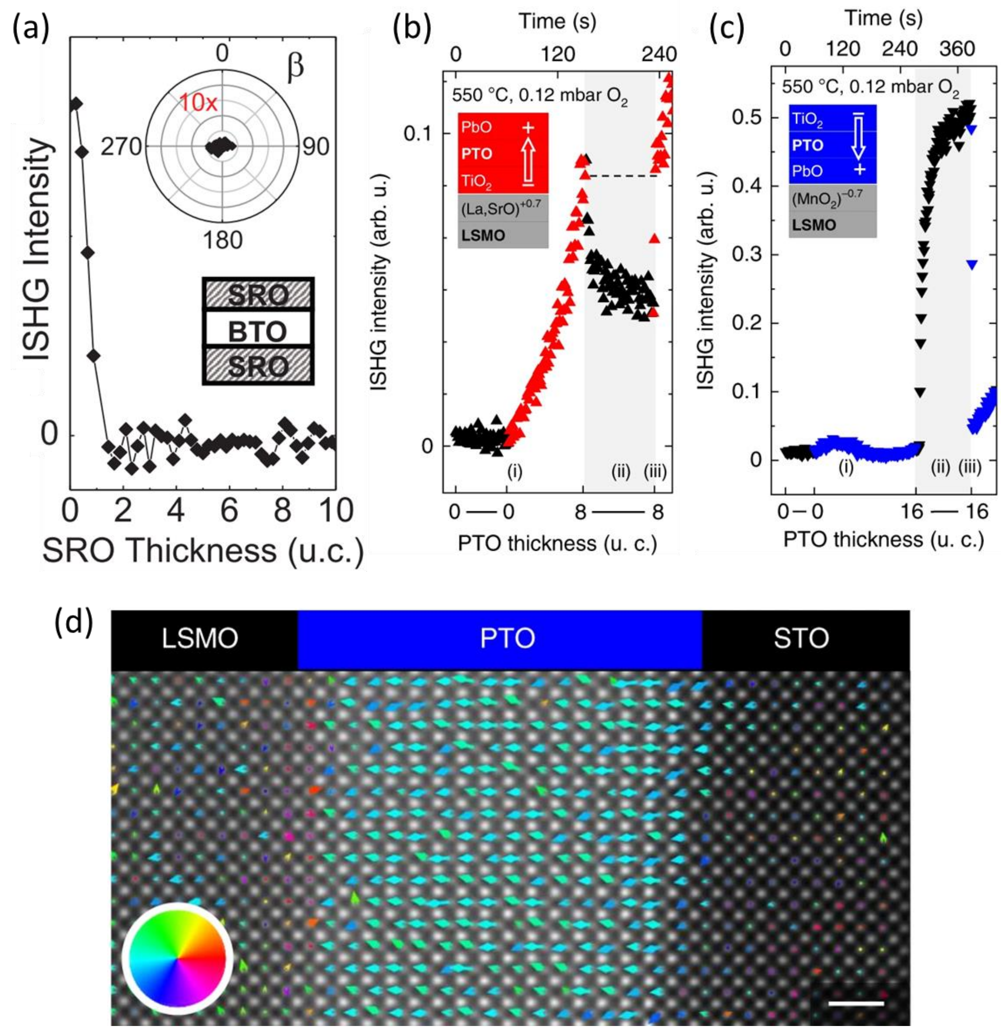

Figure 11. *(a) ISHG measurement during the deposition of the top $SrRuO_3$ (SRO) electrode on a $BaTiO_3$ (BTO) capacitor. The poor metallicity at low SRO thicknesses triggers the formation of domains and causes the ISHG drop. The inset shows the SHG anisotropy after growth. Reprinted with permission from* [30]. *Copyright 2019 by the American Physical Society. (b,c) ISHG investigations on the roles of top and bottom interface on the polarization state in $PbTiO_3$ (PTO) thin films. For competitive interactions (b) a polarization suppression is observed at growth interruption, whereas for cooperative interfaces (c) a giant polarization enhancement is found. (d) STEM map of PTO dipoles reveals a stable polarization for cooperative interfaces upon $SrTiO_3$ (STO) capping. (b-d) Reprinted from* [47].

5. Future perspectives and concluding remarks

In this section, we will discuss research directions for further avenues beyond the characterization of ferroelectrics at emergent polar interfaces and ways to in-situ probe the onset of exciting phenomena, such as the emergence of two-dimensional conducting sheets at oxide interfaces. We also share ideas towards monitoring functionalities not only in situ but also operando.

5.1 Beyond ferroelectrics: Towards the real-time observation of emerging polar interfaces

The advancement in the heteroepitaxial growth quality of transition metal oxides has eased the fabrication of oxide interfaces. Especially for strongly correlated oxides, such interfaces can host diverse exotic physical properties that cannot be observed in their bulk counterparts [222–224]. Such phenomena, including unconventional orbital and spin ordering [225,226], high-temperature superconductivity [225,227] as well as novel conducting [228,229], and polar states [230,231], hold great promise for the use of oxide interfaces as the functional component in next-generation devices. In the past decades, this potential has spurred the condensed matter research community and resulted in several excellent reviews on this topic [154,222–224,232]. Yet, despite the enormous ongoing efforts, many important questions are still under debate and new analytic tools continuously need to be developed.

Interface-sensitive optical SHG offers many advantages to deepen the understanding of the underlying processes that stand at the origin of many emergent phenomena at oxide interfaces. In particular, ISHG could provide invaluable insights into electronic reconstruction processes at interfaces. Furthermore, it becomes possible to disentangle the influence of growth parameters such as growth atmosphere and oxygen annealing procedures on the electronic states. Probably the most prominent example in the field is the two-dimensional conductive sheet at the interface between the two non-magnetic band insulators $LaAlO_3$ and $SrTiO_3$ [228]. The precise mechanism lying behind the confined conducting layer is still under debate, yet, the polar discontinuity found at the interface for $LaAlO_3$ films grown on top of $SrTiO_3$ substrates is undoubtedly a key feature. The polar discontinuity is a consequence of the stacking of neutral $(TiO_2)^0$ and $(SrO)^0$ planes in $SrTiO_3$ and charged $(AlO_2)^-$ and $(LaO)^+$ planes in $LaAlO_3$. An electric field builds up inside the $LaAlO_3$ layer and increases with thickness. This increasing instability in the $LaAlO_3$ layer is often referred to as the “polar catastrophe”. Different scenarios including charge transfer to the interface [233], cation intermixing [234–236], and oxygen vacancy mechanisms [237,238] have been proposed to avert the “polar catastrophe” and to explain the formation of the two-dimensional electron gas at a critical thickness. Several ex-situ SHG studies [239–243] on the $LaAlO_3/SrTiO_3$ system have provided information on the distinct electronic transitions involved in the electronic reconstruction that cause the conductivity, however, it was never possible to fully unravel the responsible mechanism. To that end, ISHG might add another piece to the puzzle. Monitoring the optical signature of the polar interface during its emergence as the $LaAlO_3/SrTiO_3$ system is grown or during post-growth annealing might shed light on the involved mechanism.

5.2 Operando characterization

Similarly to in-situ investigations, monitoring polarization states in the presence of external fields during device operation necessitates the development of non-invasive operando tools that enable accessing and studying changes in the performance-relevant physical properties in the active ferroelectric-based components. Such operando techniques provide information on changes in structural characteristics, meso- and microscopic domain architectures, dielectric susceptibilities, and ferroelectric polarization. Furthermore, when a high temporal resolution is available, operando tools allow the study of the intricate details of dynamics in ferroelectrics with insights into transient effects and switching timescales. As discussed in the Section 3, XRD and optical SHG are ideal non-invasive techniques suited for operando use.

Time-resolved synchrotron XRD has previously been applied to investigate structural changes in response to static and dynamic electric fields originating from domain wall motion [244] or polarization switching [245–247] in PZT and $BaTiO_3$ films. Zubko *et al.* [126] studied the response of ordered 180° ferroelectric nanodomains in $PbTiO_3/SrTiO_3$ superlattices to uniform electric fields via laboratory-scale XRD. The satellite peak intensities corresponding to the domain ordering decreases with increasing bias voltage without changes in the peak positions, as shown in Figure 12(a). This implies a change in the size of oppositely polarized domains without a change in domain periodicity, i.e. only local microscopic motion of domain walls within each domain period. Subsequent time-resolved diffraction experiments on superlattices [248,249] were used to quantify the nanosecond timescales for changes of the domain population under electrical bias.

Similar time-resolved XRD techniques have recently been used to investigate domain dynamics under radiation in $BaTiO_3$ at GHz frequency [250] and THz frequency [251]. Here, the pulsed electric field from the radiation induces a structural response, which in turn sets polarization dynamics into action and can be tracked by the operando X-ray technique.

Nonlinear optical probing offers an alternative as an operando tool to synchrotron-based techniques without relying on large-scale facilities. Mishina *et al.* [252] used SHG to study the switching dynamics in thin films of $Ba(SrTi)O_3$ upon application of in-plane oriented voltage pulses. The dynamic of the polarization reversal can be followed in the nanosecond range, as shown in Figure 12(b). SHG can be further used under various biasing conditions [253] and is even applicable as an operando probe for symmetry changes under optical excitation [254].

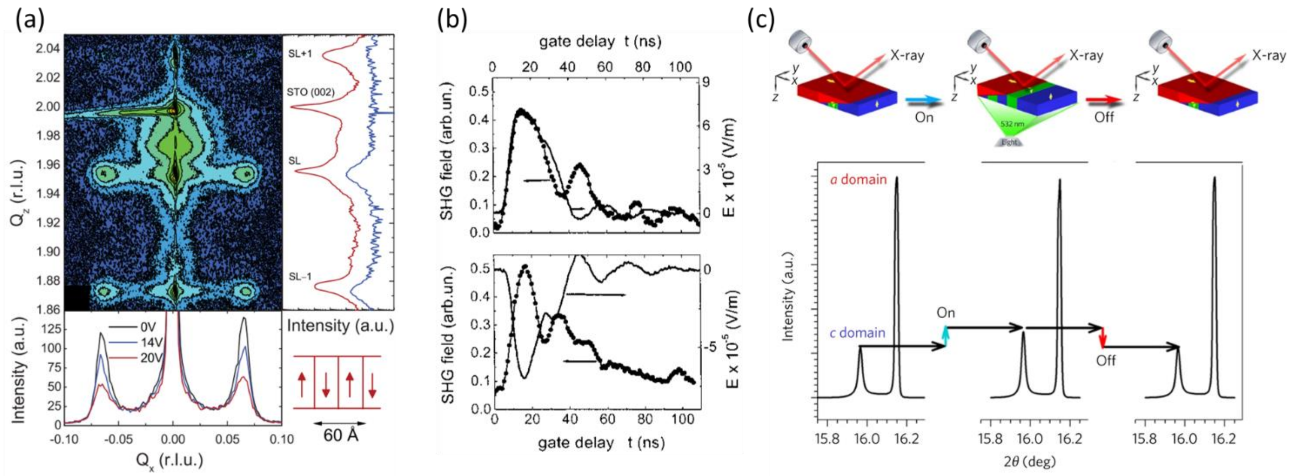

Figure 12. *(a) Reciprocal space map for a $PbTiO_3/SrTiO_3$ superlattice (SL) around the $SrTiO_3$ (002) peak. The intensity profile around the main superlattice peak (bottom) for varying electric fields shows a decreasing satellite peak intensity with increasing electric field due to domain wall motion. Reprinted with permission from* [126]*. Copyright 2010 by the American Physical Society. (b) SHG transients measured on a $Ba(Sr,Ti)O_3$ films during and after the application of positive (top) and negative (bottom) electric field pulses. From* [252]*. Reprinted with permission from AIP Publishing. Copyright 2003. (c) Illustration of a synchrotron X-ray diffraction setup to investigate the effect of light irradiation on the domain structure in $BaTiO_3$ crystals (top panel). The (200)/(002) peaks (bottom panel) show a reversible increase of the c-domain contribution under 532 nm illumination as a result of light-induced domain wall motion. From* [255]*. Reprinted with permission from Springer Nature Photonics. Copyright 2017.*

Finally, when the ferroelectric switching driving force is implemented remotely, one can consider the combination of in-situ and operando investigations. Light-induced polarization changes in ferroelectric materials have been reported, where mechanisms can involve local heating [256] , screening by photo-induced charge carriers [257], photo-induced flexoelectric effect [256], bulk photovoltaic effect [258,259], or photostriction [260]. Figure 12(c) shows the optically-induced reorientation of in-plane and out-of-plane oriented domains in $BaTiO_3$ single crystals [255]. Using light to act on ferroelectrics in situ during the growth, we envision the investigation of light-matter interactions in ferroelectric films right where the functionality is coined, with the deposition of the first few unit cells. Such operando in-situ characterization during thin film design would capture the evolution of the functionality as function of thickness with unit cell accuracy and improve our understanding of the evolution of the ferroelectric properties directly from the growth chamber.

Acknowledgements

M.T. and E.G. acknowledge the Swiss National Science Foundation under Project No. 200021-188414. M.T. and M.F.S. acknowledge the Swiss National Science Foundation Spark funding CRSK-2_196061. All authors acknowledge Manfred Fiebig for financial support and the funding by EU European Research Council under Advanced Grant Program No. 694955-INSEETO.

References

[1] Scott J F and de Araujo C A 1989 Ferroelectric Memories *Science* **246** 1400–5

[2] Setter N, Damjanovic D, Eng L, Fox G, Gevorgian S, Hong S, Kingon A, Kohlstedt H, Park N Y, Stephenson G B, Stolitchnov I, Taganstev A K, Taylor D V, Yamada T and Streiffer S 2006 Ferroelectric thin films: Review of materials, properties, and applications *J. Appl. Phys.* **100** 51606

[3] Garcia V, Bibes M, Bocher L, Valencia S, Kronast F, Crassous A, Moya X, Enouz-Vedrenne S, Gloter A, Imhoff D, Deranlot C, Mathur N D, Fusil S, Bouzehouane K and Barthélémy A 2010 Ferroelectric Control of Spin Polarization *Science* **327** 1106–10

[4] Chanthbouala A, Garcia V, Cherifi R O, Bouzehouane K, Fusil S, Moya X, Xavier S, Yamada H, Deranlot C, Mathur N D, Bibes M, Barthélémy A and Grollier J 2012 A ferroelectric memristor *Nat. Mater.* **11** 860–4

[5] Strkalj N, Gradauskaite E, Nordlander J and Trassin M 2019 Design and manipulation of ferroic domains in complex oxide heterostructures *Materials* **12**

[6] Garcia V and Bibes M 2014 Ferroelectric tunnel junctions for information storage and processing *Nat. Commun.* **5** 4289

[7] Fiebig M, Lottermoser T, Meier D and Trassin M 2016 The evolution of multiferroics *Nat. Rev. Mater.* **1**

[8] Martin L W and Rappe A M 2016 Thin-film ferroelectric materials and their applications *Nat. Rev. Mater.* **2**

[9] Trassin M 2015 Low energy consumption spintronics using multiferroic heterostructures *J. Phys. Condens. Matter* **28** 33001

[10] Zhuravlev M Y, Sabirianov R F, Jaswal S S and Tsymbal E Y 2005 Giant Electroresistance in Ferroelectric Tunnel Junctions *Phys. Rev. Lett.* **94** 246802

[11] Binasch G, Grünberg P, Saurenbach F and Zinn W 1989 Enhanced magnetoresistance in layered magnetic structures with antiferromagnetic interlayer exchange *Phys. Rev. B* **39** 4828–30

[12] Baibich M N, Broto J M, Fert A, Van Dau F N, Petroff F, Etienne P, Creuzet G, Friederich A and Chazelas J 1988 Giant Magnetoresistance of (001)Fe/(001)Cr Magnetic Superlattices *Phys. Rev. Lett.* **61** 2472–5

[13] Ralph D C and Stiles M D 2008 Spin transfer torques *J. Magn. Magn. Mater.* **320** 1190–216

[14] Myers E B, Ralph D C, Katine J A, Louie R N and Buhrman R A 1999 Current-Induced Switching of Domains in Magnetic Multilayer Devices *Science* **285** 867–70

[15] Garcia V, Fusil S, Bouzehouane K, Enouz-Vedrenne S, Mathur N D, Barthélémy A and Bibes M 2009 Giant tunnel electroresistance for non-destructive readout of ferroelectric states *Nature* **460** 81–4

[16] Scott J F 2007 Multiferroic memories *Nat. Mater.* **6** 256–7

[17] Cao W and Banerjee K 2020 Is negative capacitance FET a steep-slope logic switch? *Nat. Commun.* **11** 196

[18] Salahuddin S and Datta S 2008 Use of Negative Capacitance to Provide Voltage Amplification for Low Power Nanoscale Devices *Nano Lett.* **8** 405–10

[19] Khan A I, Keshavarzi A and Datta S 2020 The future of ferroelectric field-effect transistor technology *Nat. Electron.* **3** 588–97

[20] Salahuddin S, Ni K and Datta S 2018 The era of hyper-scaling in electronics *Nat. Electron.* **1** 442–50

[21] Khan A I, Chatterjee K, Wang B, Drapcho S, You L, Serrao C, Bakaul S R, Ramesh R and Salahuddin S 2015 Negative capacitance in a ferroelectric capacitor *Nat. Mater.* **14** 182–6

[22] Íñiguez J, Zubko P, Luk'yanchuk I and Cano A 2019 Ferroelectric negative capacitance *Nat. Rev. Mater.* **4** 243–56

[23] Catalan G, Jiménez D and Gruverman A 2015 Negative capacitance detected *Nat. Mater.* **14** 137–9

[24] Thomas S 2020 Guiding the design of negative-capacitance FETs *Nat. Electron.* **3** 72

[25] Catalan G, Seidel J, Ramesh R and Scott J F 2012 Domain wall nanoelectronics *Rev. Mod. Phys.* **84** 119–56

[26] Seidel J 2019 Nanoelectronics based on topological structures *Nat. Mater.* **18** 188–90

[27] Evans D M, Garcia V, Meier D and Bibes M Domains and domain walls in multiferroics *Phys. Sci. Rev.* **5** 20190067

[28] Leo N, Bergman A, Cano A, Poudel N, Lorenz B, Fiebig M and Meier D 2015 Polarization control at spin-driven ferroelectric domain walls *Nat. Commun.* **6** 6661

[29] Lichtensteiger C, Zubko P, Stengel M, Aguado-Puente P, Triscone J-M, Ghosez P and Junquera J 2012 Ferroelectricity in Ultrathin-Film Capacitors *Oxide Ultrathin Films* (John Wiley & Sons, Ltd) pp 230–65

[30] Strkalj N, De Luca G, Campanini M, Pal S, Schaab J, Gattinoni C, Spaldin N A, Rossell M D, Fiebig M and Trassin M 2019 Depolarizing Field Effects in Epitaxial Capacitor Heterostructures *Phys. Rev. Lett.* **123** 147601

[31] Bratkovsky A M and Levanyuk A P 2000 Abrupt Appearance of the Domain Pattern and Fatigue of Thin Ferroelectric Films *Phys. Rev. Lett.* **84** 3177–80

[32] Lichtensteiger C, Fernandez-Pena S, Weymann C, Zubko P and Triscone J-M 2014 Tuning of the Depolarization Field and Nanodomain Structure in Ferroelectric Thin Films *Nano Lett.* **14** 4205–11

[33] Lichtensteiger C, Dawber M, Stucki N, Triscone J-M, Hoffman J, Yau J-B, Ahn C H, Despont L and Aebi P 2007 Monodomain to polydomain transition in ferroelectric $PbTiO_3$ thin films with La0.67Sr0.33MnO3 electrodes *Appl. Phys. Lett.* **90** 52907

[34] Duan C-G, Sabirianov R F, Mei W-N, Jaswal S S and Tsymbal E Y 2006 Interface Effect on Ferroelectricity at the Nanoscale *Nano Lett.* **6** 483–7

[35] Liu G, Chen J, Lichtensteiger C, Triscone J-M, Aguado-Puente P, Junquera J and Valanoor N 2016 Positive Effect of an Internal Depolarization Field in Ultrathin Epitaxial Ferroelectric Films *Adv. Electron. Mater.* **2** 1500288

[36] Nagarajan V, Junquera J, He J Q, Jia C L, Waser R, Lee K, Kim Y K, Baik S, Zhao T, Ramesh R, Ghosez P and Rabe K M 2006 Scaling of structure and electrical properties in ultrathin epitaxial ferroelectric heterostructures *J. Appl. Phys.* **100** 51609

[37] Tang Y L, Zhu Y L, Ma X L, Borisevich A Y, Morozovska A N, Eliseev E A, Wang W Y, Wang Y J, Xu Y B, Zhang Z D and Pennycook S J 2015 Observation of a periodic array of flux-closure quadrants in strained ferroelectric $PbTiO_3$ films *Science* **348** 547–51

[38] Yadav A K, Nelson C T, Hsu S L, Hong Z, Clarkson J D, Schlepuëtz C M, Damodaran A R, Shafer P, Arenholz E, Dedon L R, Chen D, Vishwanath A, Minor A M, Chen L Q, Scott J F, Martin L W and Ramesh R 2016 Observation of polar vortices in oxide superlattices *Nature* **530** 198–201

[39] Wang Y J, Feng Y P, Zhu Y L, Tang Y L, Yang L X, Zou M J, Geng W R, Han M J, Guo X W, Wu B and Ma X L 2020 Polar meron lattice in strained oxide ferroelectrics *Nat. Mater.* **19** 881–6

[40] Das S, Tang Y L, Hong Z, Gonçalves M A P, McCarter M R, Klewe C, Nguyen K X, Gómez-Ortiz F, Shafer P, Arenholz E, Stoica V A, Hsu S L, Wang B, Ophus C, Liu J F, Nelson C T, Saremi S, Prasad B, Mei A B, Schlom D G, Íñiguez J, García-Fernández P, Muller D A, Chen L Q, Junquera J, Martin L W and Ramesh R 2019 Observation of room-temperature polar skyrmions *Nature* **568** 368–72

[41] Junquera J and Ghosez P 2003 Critical thickness for ferroelectricity in perovskite ultrathin films *Nature* **422** 506–9

[42] Batra I P, Wurfel P and Silverman B D 1973 Phase Transition, Stability, and Depolarization Field in Ferroelectric Thin Films *Phys. Rev. B* **8** 3257–65

[43] Kopal A, Bahnik T and Fousek J 1997 Domain formation in thin ferroelectric films: The role of depolarization energy *Ferroelectrics* **202** 267–74

[44] Zubko P, Lu H, Bark C-W, Martí X, Santiso J, Eom C-B, Catalan G and Gruverman A 2017 On the persistence of polar domains in ultrathin ferroelectric capacitors *J. Phys. Condens. Matter* **29** 284001

[45] Yu P, Luo W, Yi D, Zhang J X, Rossell M D, Yang C H, You L, Singh-Bhalla G, Yang S Y, He Q, Ramasse Q M, Erni R, Martin L W, Chu Y H, Pantelides S T, Pennycook S J and Ramesh R 2012 Interface control of bulk ferroelectric polarization *Proc. Natl. Acad. Sci.* **109** 9710–5

[46] De Luca G, Strkalj N, Manz S, Bouillet C, Fiebig M and Trassin M 2017 Nanoscale design of

polarization in ultrathin ferroelectric heterostructures *Nat. Commun.* **8** 1–7

[47] Strkalj N, Gattinoni C, Vogel A, Campanini M, Haerdi R, Rossi A, Rossell M D, Spaldin N A, Fiebig M and Trassin M 2020 In-situ monitoring of interface proximity effects in ultrathin ferroelectrics *Nat. Commun.* **11** 5815

[48] Wang R V., Fong D D, Jiang F, Highland M J, Fuoss P H, Thompson C, Kolpak A M, Eastman J A, Streiffer S K, Rappe A M and Stephenson G B 2009 Reversible chemical switching of a ferroelectric film *Phys. Rev. Lett.* **102** 2–5

[49] Highland M J, Fister T T, Fong D D, Fuoss P H, Thompson C, Eastman J A, Streiffer S K and Stephenson G B 2011 Equilibrium polarization of ultrathin $PbTiO_3$ with surface compensation controlled by oxygen partial pressure *Phys. Rev. Lett.* **107** 1–5

[50] Tian Y, Wei L, Zhang Q, Huang H, Zhang Y, Zhou H, Ma F, Gu L, Meng S, Chen L Q, Nan C W and Zhang J 2018 Water printing of ferroelectric polarization *Nat. Commun.* **9**

[51] Shin J, Nascimento V B, Geneste G, Rundgren J, Plummer E W, Dkhil B, Kalinin S V and Baddorf A P 2009 Atomistic Screening Mechanism of Ferroelectric Surfaces: An In Situ Study of the Polar Phase in Ultrathin $BaTiO_3$ Films Exposed to H_2O *Nano Lett.* **9** 3720–5

[52] Domingo N, Gaponenko I, Cordero-Edwards K, Stucki N, Pérez-Dieste V, Escudero C, Pach E, Verdaguer A and Paruch P 2019 Surface charged species and electrochemistry of ferroelectric thin films *Nanoscale* **11** 17920–30

[53] Weymann C, Lichtensteiger C, Fernandez-Peña S, Naden A B, Dedon L R, Martin L W, Triscone J-M and Paruch P 2020 Full Control of Polarization in Ferroelectric Thin Films Using Growth Temperature to Modulate Defects *Adv. Electron. Mater.* **6** 2000852

[54] Sinsheimer J, Callori S J, Ziegler B, Bein B, Chinta P V, Ashrafi A, Headrick R L and Dawber M 2013 In-situ x-ray diffraction study of the growth of highly strained epitaxial $BaTiO_3$ thin films *Appl. Phys. Lett.* **103** 242904

[55] Willmott P R and Huber J R 2000 Pulsed laser vaporization and deposition *Rev. Mod. Phys.* **72** 315–28

[56] Norton D P 2006 Pulsed Laser Deposition of Complex Materials: Progress Toward Applications *Pulsed Laser Depos. Thin Film.* 1–31

[57] Valeri S and Benedetti S 2012 Synthesis and Preparation of Oxide Ultrathin Films *Oxide Ultrathin Film.* 1–26

[58] Posadas A-B, Lippmaa M, Walker F J, Dawber M, Ahn C H and Triscone J-M 2007 Growth and Novel Applicationsof Epitaxial Oxide Thin Films BT - Physics of Ferroelectrics: A Modern Perspective (Berlin, Heidelberg: Springer Berlin Heidelberg) pp 219–304

[59] MacManus-Driscoll J L, Wells M P, Yun C, Lee J-W, Eom C-B and Schlom D G 2020 New approaches for achieving more perfect transition metal oxide thin films *APL Mater.* **8** 40904

[60] Smolenskii G A, Krainik N N, Khuchua N P, Zhdanova V V and Mylnikova I E 1966 The Curie Temperature of $LiNbO_3$ *Phys. status solidi* **13** 309–14

[61] Fong D D, Stephenson G B, Streiffer S K, Eastman J A, Aucielo O, Fuoss P H and Thompson C 2004 Ferroelectricity in ultrathin perovskite films *Science* **304** 1650–3

[62] Choi K J, Biegalski M, Li Y L, Sharan A, Schubert J, Uecker R, Reiche P, Chen Y B, Pan X Q, Gopalan V, Che L Q, Schlom D C and Eom C B 2004 Enhancement of ferroelectricity in strained $BaTiO_3$ thin films *Science* **306** 1005–9

[63] Ederer C and Spaldin N A 2005 Effect of Epitaxial Strain on the Spontaneous Polarization of Thin Film Ferroelectrics *Phys. Rev. Lett.* **95** 257601

[64] Kornev I A, Bellaiche L, Bouvier P, Janolin P-E, Dkhil B and Kreisel J 2005 Ferroelectricity of Perovskites under Pressure *Phys. Rev. Lett.* **95** 196804

[65] Everhardt A S, Matzen S, Domingo N, Catalan G and Noheda B 2016 Ferroelectric Domain Structures in Low-Strain $BaTiO_3$ *Adv. Electron. Mater.* **2** 1500214

[66] Pertsev N A, Zembilgotov A G and Tagantsev A K 1998 Effect of Mechanical Boundary Conditions on Phase Diagrams of Epitaxial Ferroelectric Thin Films *Phys. Rev. Lett.* **80** 1988–91

[67] Damodaran A R, Breckenfeld E, Chen Z, Lee S and Martin L W 2014 Enhancement of Ferroelectric Curie Temperature in $BaTiO_3$ Films via Strain-Induced Defect Dipole Alignment *Adv. Mater.* **26** 6341–7

[68] Sarott M F, Fiebig M and Trassin M 2020 Tracking ferroelectric domain formation during epitaxial growth of $PbTiO_3$ films *Appl. Phys. Lett.* **117** 132901

[69] Pertsev N A, Tagantsev A K and Setter N 2000 Phase transitions and strain-induced ferroelectricity in $SrTiO_3$ epitaxial thin films *Phys. Rev. B* **61** R825--R829

[70] Haeni J H, Irvin P, Chang W, Uecker R, Reiche P, Li Y L, Choudhury S, Tian W, Hawley M E, Craigo B, Tagantsev A K, Pan X Q, Streiffer S K, Chen L Q, Kirchoefer S W, Levy J and Schlom D G 2004 Room-temperature ferroelectricity in strained $SrTiO_3$ *Nature* **430** 758–61

[71] Tyunina M, Narkilahti J, Plekh M, Oja R, Nieminen R M, Dejneka A and Trepakov V 2010 Evidence for Strain-Induced Ferroelectric Order in Epitaxial Thin-Film $KTaO_3$ *Phys. Rev. Lett.* **104** 227601

[72] Becher C, Maurel L, Aschauer U, Lilienblum M, Magén C, Meier D, Langenberg E, Trassin M, Blasco J, Krug I P, Algarabel P A, Spaldin N A, Pardo J A and Fiebig M 2015 Strain-induced coupling of electrical polarization and structural defects in $SrMnO_3$ films *Nat. Nanotechnol.* **10** 661–5

[73] Günter T, Bousquet E, David A, Boullay P, Ghosez P, Prellier W and Fiebig M 2012 Incipient ferroelectricity in 2.3% tensile-strained $CaMnO_3$ films *Phys. Rev. B* **85** 214120

[74] Gruverman A, Alexe M and Meier D 2019 Piezoresponse force microscopy and nanoferroic phenomena *Nat. Commun.* **10** 1661

[75] Rabe K M, Ahn C H and Triscone J-M 2007 *Physics of Ferroelectrics. A Modern Perspective.* (Berlin: Springer - Verlag Berlin Heidelberg)

[76] Denev S A, Lummen T T A, Barnes E, Kumar A and Gopalan V 2011 Probing ferroelectrics using optical second harmonic generation *J. Am. Ceram. Soc.* **94** 2699–727

[77] Scott J F 2008 Ferroelectrics go bananas *J. Phys. Condens. Matter* **20** 15–7

[78] Dawber M, Rabe K M and Scott J F 2005 Physics of thin-film ferroelectric oxides *Rev. Mod. Phys.* **77** 1083–130

[79] Jaffee B, Cook W R and Jaffee H 1971 *Piezoelectric Ceramics* (London: Academic Press)

[80] Scott J F 2000 *Ferroelectric Memories* (New York: Springer - Verlag Berlin Heidelberg)

[81] Noguchi Y, Matsumoto T and Miyayama M 2005 Impact of defect control on the polarization properties in $Bi_4Ti_3O_{12}$ ferroelectric single crystals *Jpn. J. Appl. Phys.* **44** L570

[82] Gradauskaite E, Gardner J, Smith R M, Morrison F D, Lee S L, Katiyar R S and Scott J F 2017 Lead palladium titanate: A room-temperature multiferroic *Phys. Rev. B* **96** 104104

[83] Yan H, Inam F, Viola G, Ning H, Zhang H, Jiang Q, Zeng T, Gao Z and Reece M J 2011 the Contribution of Electrical Conductivity, Dielectric Permittivity and Domain Switching in Ferroelectric Hysteresis Loops *J. Adv. Dielectr.* **01** 107–18

[84] Kim D J, Jo J Y, Kim Y S, Chang Y J, Lee J S, Yoon J G, Song T K and Noh T W 2005 Polarization relaxation induced by a depolarization field in ultrathin ferroelectric $BaTiO_3$ capacitors *Phys. Rev. Lett.* **95** 237602

[85] Naganuma H, Inoue Y and Okamura S 2008 Evaluation of electrical properties of leaky $BiFeO_3$ films in high electric field region by high-speed positive-up-negative-down measurement *Appl. Phys. Express* **1** 061601

[86] Fina I, Fàbrega L, Langenberg E, Martí X, Sánchez F, Varela M and Fontcuberta J 2011 Nonferroelectric contributions to the hysteresis cycles in manganite thin films: A comparative study of measurement techniques *J. Appl. Phys.* **109** 74105

[87] Meyer R, Waser R, Prume K, Schmitz T and Tiedke S 2005 Dynamic leakage current compensation in ferroelectric thin-film capacitor structures *Appl. Phys. Lett.* **86** 142907

[88] Pintilie L and Alexe M 2005 Metal-ferroelectric-metal heterostructures with Schottky contacts. I. Influence of the ferroelectric properties *J. Appl. Phys.* **98** 124103

[89] Pintilie L and Alexe M 2005 Ferroelectric-like hysteresis loop in nonferroelectric systems *Appl. Phys. Lett.* **87** 8–11

[90] Hubmann A H, Li S, Zhukov S, Von Seggern H and Klein A 2016 Polarisation dependence of Schottky barrier heights at ferroelectric $BaTiO_3$ / RuO_2 interfaces: Influence of substrate orientation and quality *J. Phys. D. Appl. Phys.* **49** 295304

[91] Brennan C 1993 Model of ferroelectric fatigue due to defect/domain interactions *Ferroelectrics* **150** 199–208

[92] Warren W L, Tuttle B A and Dimos D 1995 Ferroelectric fatigue in perovskite oxides *Appl. Phys. Lett.* **67** 1426

[93] Dawber M and Scott J F 2000 A model for fatigue in ferroelectric perovskite thin films *Appl. Phys. Lett.* **76** 1060–2

[94] Damodaran A R, Agar J C, Pandya S, Chen Z, Dedon L, Xu R, Apgar B, Saremi S and Martin L W 2016 New modalities of strain-control of ferroelectric thin films *J. Phys. Condens. Matter* **28**

263001

[95] Ramesh R and Keramidas V G 1995 Metal-Oxide Heterostructures *Annu. Rev. Mater. Sci.* **25** 647–78

[96] Pintilie L, Vrejoiu I, Hesse D and Alexe M 2008 The influence of the top-contact metal on the ferroelectric properties of epitaxial ferroelectric $Pb(Zr_{0.2}Ti_{0.8})O_3$ thin films *J. Appl. Phys.* **104** 114101

[97] Kalinin S V., Rodriguez B J, Jesse S, Chu Y H, Zhao T, Ramesh R, Choudhury S, Chen L Q, Eliseev E A and Morozovska A N 2007 Intrinsic single-domain switching in ferroelectric materials on a nearly ideal surface *Proc. Natl. Acad. Sci.* **104** 20204–9

[98] Gruverman A, Wu D and Scott J F 2008 Piezoresponse force microscopy studies of switching behavior of ferroelectric capacitors on a 100-ns time scale *Phys. Rev. Lett.* **100** 3–6

[99] Jesse S, Lee H N and Kalinin S V. 2006 Quantitative mapping of switching behavior in piezoresponse force microscopy *Rev. Sci. Instrum.* **77** 073702

[100] Gruverman A, Wu D, Fan H J, Vrejoiu I, Alexe M, Harrison R J and Scott J F 2008 Vortex ferroelectric domains *J. Phys. Condens. Matter* **20** 342201

[101] Zhang Q, Xie L, Liu G, Prokhorenko S, Nahas Y, Pan X, Bellaiche L, Gruverman A and Valanoor N 2017 Nanoscale Bubble Domains and Topological Transitions in Ultrathin Ferroelectric Films *Adv. Mater.* **29** 1702375

[102] Gruverman A and Kalinin S V 2006 Piezoresponse force microscopy and recent advances in nanoscale studies of ferroelectrics *J. Mater. Sci.* **41** 107–16

[103] Steffes J J, Ristau R A, Ramesh R and Huey B D 2019 Thickness scaling of ferroelectricity in $BiFeO_3$ by tomographic atomic force microscopy *Proc. Natl. Acad. Sci.* **116** 2413–8

[104] Balke N, Maksymovych P, Jesse S, Herklotz A, Tselev A, Eom C B, Kravchenko I I, Yu P and Kalinin S V. 2015 Differentiating Ferroelectric and Nonferroelectric Electromechanical Effects with Scanning Probe Microscopy *ACS Nano* **9** 6484–92

[105] Seol D, Kim B and Kim Y 2017 Non-piezoelectric effects in piezoresponse force microscopy *Curr. Appl. Phys.* **17** 661–74

[106] Urban K W 2008 Studying atomic structures by aberration-corrected transmission electron microscopy *Science* **321** 506–10

[107] Wu H, Zhao X, Song D, Tian F, Wang J, Loh K P and Pennycook S J 2018 Progress and prospects of aberration-corrected STEM for functional materials *Ultramicroscopy* **194** 182–92

[108] Mayer J, Giannuzzi L a, Kamino T and Michael J 2007 TEM Sample Preparation and Damage *MRS Bull.* **32** 400–7

[109] Li C, Habler G, Baldwin L C and Abart R 2018 An improved FIB sample preparation technique for site-specific plan-view specimens: A new cutting geometry *Ultramicroscopy* **184** 310–7

[110] Mosberg A B, Roede E D, Evans D M, Holstad T S, Bourret E, Yan Z, Van Helvoort A T J and Meier D 2019 FIB lift-out of conducting ferroelectric domain walls in hexagonal manganites *Appl. Phys.*

Lett. **115** 122901

[111] Erni R, Rossell M D, Kisielowski C and Dahmen U 2009 Atomic-Resolution Imaging with a Sub-50-pm Electron Probe *Phys. Rev. Lett.* **102** 96101

[112] Schilling A, Adams T B, Bowman R M, Gregg J M, Catalan G and Scott J F 2006 Scaling of domain periodicity with thickness measured in $BaTiO_3$ single crystal lamellae and comparison with other ferroics *Phys. Rev. B* **74** 24115

[113] Wei X K, Jia C L, Sluka T, Wang B X, Ye Z G and Setter N 2016 Néel-like domain walls in ferroelectric $Pb(Zr,Ti)O_3$ single crystals *Nat. Commun.* **7** 12385

[114] De Luca G, Rossell M D, Schaab J, Viart N, Fiebig M and Trassin M 2017 Domain Wall Architecture in Tetragonal Ferroelectric Thin Films *Adv. Mater.* **29** 1–5

[115] Nelson C T, Winchester B, Zhang Y, Kim S J, Melville A, Adamo C, Folkman C M, Baek S H, Eom C B, Schlom D G, Chen L Q and Pan X 2011 Spontaneous vortex nanodomain arrays at ferroelectric heterointerfaces *Nano Lett.* **11** 828–34

[116] Schilling A, Byrne D, Catalan G, Webber K G, Genenko Y A, Wu G S, Scott J F and Gregg J M 2009 Domains in Ferroelectric Nanodots *Nano Lett.* **9** 3359–64

[117] Campanini M, Trassin M, Ederer C, Erni R and Rossell M D 2019 Buried In-Plane Ferroelectric Domains in Fe-Doped Single-Crystalline Aurivillius Thin Films *ACS Appl. Electron. Mater.* **1** 1019–28

[118] Nordlander J, Campanini M, Rossell M D, Erni R, Meier Q N, Cano A, Spaldin N A, Fiebig M and Trassin M 2019 The ultrathin limit of improper ferroelectricity *Nat. Commun.* **10** 5591

[119] Campanini M, Erni R and Rossell M D Probing local order in multiferroics by transmission electron microscopy *Phys. Sci. Rev.* **5** 20190068

[120] Erni R 2015 *Aberration-corrected imaging in transmission electron microscopy: An introduction second edition* (Imperial College Press)

[121] Shibata N, Seki T, Sánchez-Santolino G, Findlay S D, Kohno Y, Matsumoto T, Ishikawa R and Ikuhara Y 2017 Electric field imaging of single atoms *Nat. Commun.* **8** 15631

[122] Fong D D and Thompson C 2006 In situ synchrotron X-ray studies of ferroelectric thin films *Annu. Rev. Mater. Res.* **36** 431–65

[123] Nordlander J, De Luca G, Strkalj N, Fiebig M and Trassin M 2018 Probing ferroic states in oxide thin films using optical second harmonic generation *Appl. Sci.* **8**

[124] Fiebig M, Pavlov V V. and Pisarev R V. 2005 Second-harmonic generation as a tool for studying electronic and magnetic structures of crystals: review *J. Opt. Soc. Am. B* **22** 96

[125] Lichtensteiger C, Triscone J-M, Junquera J and Ghosez P 2005 Ferroelectricity and Tetragonality in Ultrathin $PbTiO_3$ Films *Phys. Rev. Lett.* **94** 47603

[126] Zubko P, Stucki N, Lichtensteiger C and Triscone J-M 2010 X-Ray Diffraction Studies of 180° Ferroelectric Domains in $PbTiO_3/SrTiO_3$ Superlattices under an Applied Electric Field *Phys. Rev. Lett.* **104** 187601

[127] Chen Z H, Damodaran A R, Xu R, Lee S and Martin L W 2014 Effect of “symmetry mismatch” on the domain structure of rhombohedral $BiFeO_3$ thin films *Appl. Phys. Lett.* **104** 182908

[128] Heron J T, Schlom D G and Ramesh R 2014 Electric field control of magnetism using $BiFeO_3$-based heterostructures *Appl. Phys. Rev.* **1** 21303

[129] Chu Y-H, He Q, Yang C-H, Yu P, Martin L W, Shafer P and Ramesh R 2009 Nanoscale Control of Domain Architectures in $BiFeO_3$ Thin Films *Nano Lett.* **9** 1726–30

[130] Chu Y-H, Cruz M P, Yang C-H, Martin L W, Yang P-L, Zhang J-X, Lee K, Yu P, Chen L-Q and Ramesh R 2007 Domain Control in Multiferroic $BiFeO_3$ through Substrate Vicinality *Adv. Mater.* **19** 2662–6

[131] Khan A I, Yu P, Trassin M, Lee M J, You L and Salahuddin S 2014 The effects of strain relaxation on the dielectric properties of epitaxial ferroelectric $Pb(Zr_{0.2}Ti_{0.8})TiO_3$ thin films *Appl. Phys. Lett.* **105** 22903

[132] Nordlander J, Eltes F, Reynaud M, Nürnberg J, De Luca G, Caimi D, Demkov A A, Abel S, Fiebig M, Fompeyrine J and Trassin M 2020 Ferroelectric domain architecture and poling of $BaTiO_3$ on Si *Phys. Rev. Mater.* **4** 34406

[133] Zubko P, Jecklin N, Torres-Pardo A, Aguado-Puente P, Gloter A, Lichtensteiger C, Junquera J, Stéphan O and Triscone J-M 2012 Electrostatic Coupling and Local Structural Distortions at Interfaces in Ferroelectric/Paraelectric Superlattices *Nano Lett.* **12** 2846–51

[134] Streiffer S K, Eastman J A, Fong D D, Thompson C, Munkholm A, Ramana Murty M V, Auciello O, Bai G R and Stephenson G B 2002 Observation of Nanoscale 180° Stripe Domains in Ferroelectric $PbTiO_3$ Thin Films *Phys. Rev. Lett.* **89** 67601

[135] Lefevre C, Demchenko A, Bouillet C, Luysberg M, Devaux X, Roulland F, Versini G, Barre S, Wakabayashi Y, Boudet N, Leuvrey C, Acosta M, Meny C, Martin E, Grenier S, Favre-Nicolin V and Viart N 2017 Nondestructive Method for the Determination of the Electric Polarization Orientation in Thin Films: Illustration on Gallium Ferrite Thin Films *Small Methods* **1** 1700234

[136] Gorfman S, Simons H, Iamsasri T, Prasertpalichat S, Cann D P, Choe H, Pietsch U, Watier Y and Jones J L 2016 Simultaneous resonant x-ray diffraction measurement of polarization inversion and lattice strain in polycrystalline ferroelectrics *Sci. Rep.* **6** 20829

[137] Shen Y R 1986 Surface Second Harmonic Generation: A New Technique for Surface Studies *Annu. Rev. Mater. Sci.* **16** 69–86

[138] Kaneshiro J, Uesu Y and Fukui T 2010 Visibility of inverted domain structures using the second harmonic generation microscope: Comparison of interference and non-interference cases *J. Opt. Soc. Am. B* **27** 888–94

[139] Matsubara M, Manz S, Mochizuki M, Kubacka T, Iyama A, Aliouane N, Kimura T, Johnson S L, Meier D and Fiebig M 2015 Magnetoelectric domain control in multiferroic $TbMnO_3$ *Science* **348** 1112–5

[140] Lummen T T A, Gu Y, Wang J, Lei S, Xue F, Kumar A, Barnes A T, Barnes E, Denev S, Belianinov A, Holt M, Morozovska A N, Kalinin S V, Chen L-Q and Gopalan V 2014 Thermotropic phase boundaries in classic ferroelectrics *Nat. Commun.* **5** 3172

[141] Kumar A, Denev S, Zeches R J, Vlahos E, Podraza N J, Melville A, Schlom D G, Ramesh R and Gopalan V 2010 Probing mixed tetragonal/rhombohedral-like monoclinic phases in strained bismuth ferrite films by optical second harmonic generation *Appl. Phys. Lett.* **97** 112903

[142] Trassin M, Luca G De, Manz S and Fiebig M 2015 Probing Ferroelectric Domain Engineering in $BiFeO_3$ Thin Films by Second Harmonic Generation *Adv. Mater.* **27** 4871–6

[143] Yokota H and Uesu Y 2021 Optical second-harmonic generation microscopy as a tool for ferroelastic domain wall exploration *J. Appl. Phys.* **129** 14101

[144] Janz S, Bottomley D J, van Driel H M and Timsit R S 1991 Influence of steps on second-harmonic generation from vicinal metal surfaces *Phys. Rev. Lett.* **66** 1201–4

[145] Murphy R, Yeganeh M, Song K J and Plummer E W 1989 Second-harmonic generation from the surface of a simple metal, Al *Phys. Rev. Lett.* **63** 318–21

[146] Heinz T F, Loy M M T and Thompson W A 1985 Study of Si(111) Surfaces by Optical Second-Harmonic Generation: Reconstruction and Surface Phase Transformation *Phys. Rev. Lett.* **54** 63–6

[147] Coy E, Graczyk P, Yate L, Załęski K, Gapiński J, Kuświk P, Mielcarek S, Stobiecki F, Mróz B, Ferrater C and Jurga S 2017 Second Harmonic Generation Response in Thermally reconstructed Multiferroic β′- $Gd_2(MoO_4)_3$ Thin Films *Sci. Rep.* **7** 11800

[148] Reif J, Tepper P, Matthias E, Westin E and Rosén A 1988 Surface structure of cubic ionic crystals studied by optical second-harmonic generation *Appl. Phys. B* **46** 131–8

[149] Yokota H, Haines C R S, Matsumoto S, Hasegawa N, Carpenter M A, Heo Y, Marin A, Salje E K H and Uesu Y 2020 Domain wall generated polarity in ferroelastics: Results from resonance piezoelectric spectroscopy, piezoelectric force microscopy, and optical second harmonic generation measurements in $LaAlO_3$ with twin and tweed microstructures *Phys. Rev. B* **102** 104117

[150] Zhang Y, Zhang Y, Guo Q, Zhong X, Chu Y, Lu H, Zhong G, Jiang J, Tan C, Liao M, Lu Z, Zhang D, Wang J, Yuan J and Zhou Y 2018 Characterization of domain distributions by second harmonic generation in ferroelectrics *npj Comput. Mater.* **4** 39

[151] Cherifi-Hertel S, Bulou H, Hertel R, Taupier G, Dorkenoo K D H, Andreas C, Guyonnet J, Gaponenko I, Gallo K and Paruch P 2017 Non-Ising and chiral ferroelectric domain walls revealed by nonlinear optical microscopy *Nat. Commun.* **8** 1–9

[152] De Luca G, Schoenherr P, Mendil J, Meier D, Fiebig M and Trassin M 2018 Domain-Pattern Transfer across an Artificial Magnetoelectric Interface *Phys. Rev. Appl.* **10** 54030

[153] Spaldin N A and Ramesh R 2019 Advances in magnetoelectric multiferroics *Nat. Mater.* **18** 203–12

[154] Coll M, Fontcuberta J, Althammer M, Bibes M, Boschker H, Calleja A, Cheng G, Cuoco M, Dittmann R, Dkhil B, El Baggari I, Fanciulli M, Fina I, Fortunato E, Frontera C, Fujita S, Garcia V, Goennenwein S T B, Granqvist C G, Grollier J, Gross R, Hagfeldt A, Herranz G, Hono K, Houwman E, Huijben M, Kalaboukhov A, Keeble D J, Koster G, Kourkoutis L F, Levy J, Lira-Cantu M, MacManus-Driscoll J L, Mannhart J, Martins R, Menzel S, Mikolajick T, Napari M, Nguyen M D, Niklasson G, Paillard C, Panigrahi S, Rijnders G, Sánchez F, Sanchis P, Sanna S, Schlom D G, Schroeder U, Shen K

M, Siemon A, Spreitzer M, Sukegawa H, Tamayo R, van den Brink J, Pryds N and Granozio F M 2019 Towards Oxide Electronics: a Roadmap *Appl. Surf. Sci.* **482** 1–93

[155] Price G L 2003 Reflection High Energy Electron Diffraction *Surface Analysis Methods in Materials Science* ed D J O'Connor (Berlin: Springer - Verlag Berlin Heidelberg) pp 307–18

[156] Rubi D, Vlooswijk A H G and Noheda B 2009 Growth of flat $SrRuO_3$ (111) thin films suitable as bottom electrodes in heterostructures *Thin Solid Films* **517** 1904–7

[157] Osten H J and Klatt J 1994 In situ monitoring of strain relaxation during antimony-mediated growth of Ge and Ge1−y Cy layers on Si(001) using reflection high energy electron diffraction *Appl. Phys. Lett.* **65** 630–2

[158] Soukiassian A, Tian W, Vaithyanathan V, Haeni J H, Chen L Q, Xi X X, Schlom D G, Tenne D A, Sun H P, Pan X Q, Choi K J, Eom C B, Li Y L, Jia Q X, Constantin C, Feenstra R M, Bernhagen M, Reiche P and Uecker R 2008 Growth of nanoscale $BaTiO_3$/$SrTiO_3$ superlattices by molecular-beam epitaxy *J. Mater. Res.* **23** 1417–32

[159] Braun W 1999 MBE-grown semiconductor interfaces *Applied RHEED Reflection High-Energy Electron Diffraction During Crystal Growth* (Berlin: Springer - Verlag Berlin Heidelberg) pp 1–11

[160] Tsui D C, Stormer H L and Gossard A C 1982 Two-dimensional magnetotransport in the extreme quantum limit *Phys. Rev. Lett.* **48** 1559–62

[161] Melloch M R 1993 Molecular beam epitaxy for high electron mobility modulation-doped two-dimensional electron gases *Thin Solid Films* **231** 74–85

[162] Pfeiffer L N, West K W, Willett R L, Akiyama H and Rokhinson L P 2005 Nanostructures in GaAs fabricated by molecular beam epitaxy *Bell Syst. Tech. J.* **10** 151–9

[163] Chen P, Kim J Y, Madhukar A and Cho N M 1986 Optimal surface and growth front of III–V semiconductors in molecular beam epitaxy: A study of kinetic processes via reflection high energy electron diffraction specular beam intensity measurements on GaAs(100) *J. Vac. Sci. Technol. B* **4** 890–5

[164] Mundy J A, Brooks C M, Holtz M E, Moyer J A, Das H, Rébola A F, Heron J T, Clarkson J D, Disseler S M, Liu Z, Farhan A, Held R, Hovden R, Padgett E, Mao Q, Paik H, Misra R, Kourkoutis L F, Arenholz E, Scholl A, Borchers J A, Ratcliff W D, Ramesh R, Fennie C J, Schiffer P, Muller D A and Schlom D G 2016 Atomically engineered ferroic layers yield a room-temperature magnetoelectric multiferroic *Nature* **537** 523–7

[165] Nie Y F, Zhu Y, Lee C H, Kourkoutis L F, Mundy J A, Junquera J, Ghosez P, Baek D J, Sung S, Xi X X, Shen K M, Muller D A and Schlom D G 2014 Atomically precise interfaces from non-stoichiometric deposition *Nat. Commun.* **5** 4530

[166] Rijnders A J H M 2001 *The initial growth of complex oxides : study and manipulation* (Netherlands: University of Twente)

[167] Podkaminer J P, Patzner J J, Davidson B A and Eom C B 2016 Real-time and in situ monitoring of sputter deposition with RHEED for atomic layer controlled growth *APL Mater.* **4** 86111

[168] Frank F C and Van Der Merwe J H 1949 One-dimensional dislocations . I. Static theory *Proc. R.*

Soc. A **198** 205–16

[169] Solmaz A, Huijben M, Koster G, Egoavil R, Gauquelin N, Van Tendeloo G, Verbeeck J, Noheda B and Rijnders G 2016 Domain Selectivity in $BiFeO_3$ Thin Films by Modified Substrate Termination *Adv. Funct. Mater.* **26** 2882–9

[170] Guo R, Shen L, Wang H, Lim Z, Lu W, Yang P, Ariando, Gruverman A, Venkatesan T, Feng Y P and Chen J 2016 Tailoring Self-Polarization of $BaTiO_3$ Thin Films by Interface Engineering and Flexoelectric Effect *Adv. Mater. Interfaces* **3** 1600737

[171] Lee H G, Wang L, Si L, He X, Porter D G, Kim J R, Ko E K, Kim J, Park S M, Kim B, Wee A T S, Bombardi A, Zhong Z and Noh T W 2020 Atomic-Scale Metal–Insulator Transition in $SrRuO_3$ Ultrathin Films Triggered by Surface Termination Conversion *Adv. Mater.* **32** 1905815

[172] Rijnders G, Blank D H A, Choi J and Eom C B 2004 Enhanced surface diffusion through termination conversion during epitaxial $SrRuO_3$ growth *Appl. Phys. Lett.* **84** 505–7

[173] Sánchez F, Ocal C and Fontcuberta J 2014 Tailored surfaces of perovskite oxide substrates for conducted growth of thin films *Chem. Soc. Rev.* **43** 2272–85

[174] Takahashi R, Matsumoto Y, Ohsawa T, Lippmaa M, Kawasaki M and Koinuma H 2002 Growth dynamics of the epitaxial SrO film on $SrTiO_3$(001) *J. Cryst. Growth* **234** 505–8

[175] Koster G, Huijben M, Janssen A and Rijnders G 2015 *Growth studies of heteroepitaxial oxide thin films using reflection high-energy electron diffraction (RHEED)* vol 1 (Elsevier Ltd)

[176] Gradauskaite E, Campanini M, Biswas B, Schneider C W, Fiebig M, Rossell M D and Trassin M 2020 Robust In-Plane Ferroelectricity in Ultrathin Epitaxial Aurivillius Films *Adv. Mater. Interfaces* **2000202** 1–8

[177] Nordlander J, Rossell M D, Campanini M, Fiebig M and Trassin M 2020 Epitaxial integration of improper ferroelectric hexagonal $YMnO_3$ thin films in heterostructures *Phys. Rev. Mater.* **4** 124403

[178] Homkar S, Preziosi D, Devaux X, Bouillet C, Nordlander J, Trassin M, Roulland F, Lefèvre C, Versini G, Barre S, Leuvrey C, Lenertz M, Fiebig M, Pourroy G and Viart N 2019 Ultrathin regime growth of atomically flat multiferroic gallium ferrite films with perpendicular magnetic anisotropy *Phys. Rev. Mater.* **3** 124416

[179] Trassin M, Viart N, Versini G, Barre S, Pourroy G, Lee J, Jo W, Dumesnil K, Dufour C and Robert S 2009 Room temperature ferrimagnetic thin films of the magnetoelectric $Ga_{2-x}Fe_xO_3$ *J. Mater. Chem.* **19** 8876–80

[180] Gallon T E and Matthew J A D 1972 Auger electron spectroscopy and its application to surface studies *Rev. Phys. Technol.* **3** 31–64

[181] Debehets J, Miranda S M C, Homm P, Houssa M, Seefeldt M, Locquet J-P and Seo J W 2016 Auger electron spectroscopy study of semiconductor surfaces: Effect of cleaning in inert atmosphere *J. Vac. Sci. Technol. B* **34** 041227

[182] Orvis T, Surendran M, Liu Y, Cunniff A and Ravichandran J 2019 In situ Auger electron spectroscopy of complex oxide surfaces grown by pulsed laser deposition *J. Vac. Sci. Technol. A*

37 061401

[183] Singh-Bhalla G, Rossen P B, Pálsson G K, Mecklenburg M, Orvis T, Das S, Tang Y L, Suresha J S, Yi D, Dasgupta A, Doenning D, Ruiz V G, Yadav A K, Trassin M, Heron J T, Fadley C S, Pentcheva R, Ravichandran J and Ramesh R 2018 Unexpected termination switching and polarity compensation in $LaAlO_3/SrTiO_3$ heterostructures *Phys. Rev. Mater.* **2** 1–7

[184] Hilfiker J N 2011 In situ spectroscopic ellipsometry (SE) for characterization of thin film growth *In Situ Characterization of Thin Film Growth* ed G Koster and G Rijnders (Cambridge: Woodhead Publishing Limited) pp 99–151

[185] Langereis E, Heil S B S, Knoops H C M, Keuning W, Van De Sanden M C M and Kessels W M M 2009 In situ spectroscopic ellipsometry as a versatile tool for studying atomic layer deposition *J. Phys. D. Appl. Phys.* **42** 073001

[186] Jellison G E 1998 Spectroscopic ellipsometry data analysis: Measured versus calculated quantities *Thin Solid Films* **313**–**314** 33–9

[187] Trolier-McKinstry S, Chen J, Vedam K and Newnham R E 1995 In Situ Annealing Studies of Sol-Gel Ferroelectric Thin Films by Spectroscopic Ellipsometry *J. Am. Ceram. Soc.* **78** 1907

[188] Singh D J, Seo S S A and Lee H N 2010 Optical properties of ferroelectric $Bi_4Ti_3O_{12}$ *Phys. Rev. B.* **82** 3–6

[189] Bahng J H, Lee M, Park H L, Won K, Jeong J H and Kim K J 2001 Spectroscopic ellipsometry study of $SrBi_2Ta_2O_9$ ferroelectric thin films *Appl. Phys. Lett.* **79** 1664–6

[190] Hu Z, Wang G, Huang Z, Meng X, Shi F and Chu J 2003 Investigations of the Optical Properties of $Ba_{0.9}Sr_{0.1}TiO_3$ Ferroelectric Thin Films by Spectroscopic Ellipsometry *Jpn. J. Appl. Phys.* **42** 1400–4

[191] Kumar A, Rai R C, Podraza N J, Denev S, Ramirez M, Chu Y H, Martin L W, Ihlefeld J, Heeg T, Schubert J, Schlom D G, Orenstein J, Ramesh R, Collins R W, Musfeldt J L and Gopalan V 2008 Linear and nonlinear optical properties of $BiFeO_3$ *Appl. Phys. Lett.* **92** 121915

[192] Hu Z G, Li Y W, Zhu M, Zhu Z Q and Chu J H 2008 Microstructural and optical investigations of sol-gel derived ferroelectric $BaTiO_3$ nanocrystalline films determined by spectroscopic ellipsometry *Phys. Lett. Sect. A Gen. At. Solid State Phys.* **372** 4521–6

[193] Zhang J Z, Jiang K, Hu Z G and Chu J H 2016 A novel technique for probing phase transitions in ferroelectric functional materials: Condensed matter spectroscopy *Sci. China Technol. Sci.* **59** 1537–48

[194] Železný V, Chvostová D, Šimek D, Máca F, Mašek J, Setter N and Hong Huang Y 2016 The variation of $PbTiO_3$ bandgap at ferroelectric phase transition *J. Phys. Condens. Matter* **28** 025501

[195] Pascual-Gonzalez C, Schileo G and Feteira A 2016 Band gap narrowing in ferroelectric $KNbO_3$-$Bi(Yb,Me)O_3$ (Me=Fe or Mn) ceramics *Appl. Phys. Lett.* **109** 3–8

[196] Tyunina M, Dejneka A, Chvostova D, Levoska J, Plekh M and Jastrabik L 2012 Phase transitions in ferroelectric $Pb_{0.5}Sr_{0.5}TiO_3$ films probed by spectroscopic ellipsometry *Phys. Rev. B* **86** 224105

[197] Kondo S, Yamada T, Tagantsev A K, Ma P, Leuthold J, Martelli P, Boffi P, Martinelli M, Yoshino M

and Nagasaki T 2019 Large impact of strain on the electro-optic effect in (Ba,Sr)TiO_3 thin films: Experiment and theoretical comparison *Appl. Phys. Lett.* **115** 092901

[198] Lei D Y, Kéna-Cohen S, Zou B, Petrov P K, Sonnefraud Y, Breeze J, Maier S A and Alford N M 2012 Spectroscopic ellipsometry as an optical probe of strain evolution in ferroelectric thin films *Opt. Express* **20** 4419

[199] Jha R K, Singh P, Goswami M and Singh B R 2019 Comparative study of structural electrical dielectric and ferroelectric properties of HfO_2 deposited by plasma-enhanced atomic layer deposition and radio frequency sputtering technique for the application in 1-T FeFET *J. Mater. Sci. Mater. Electron.* **30** 20360–8

[200] Lyzwa F, Marsik P, Roddatis V, Bernhard C, Jungbauer M and Moshnyaga V 2018 In situ monitoring of atomic layer epitaxy via optical ellipsometry *J. Phys. D. Appl. Phys.* **51** 125306

[201] Jähnke V, Conrad U, Güdde J and Matthias E 1999 SHG investigations of the magnetization of thin Ni and Co films on Cu(001) *Appl. Phys. B* **68** 485–9

[202] Weschke E, Schüssler-Langeheine C, Meier R, Kaindl G, Sutter C, Abernathy D and Grübel G 1997 q Dependence of the Growth-Oscillation Period of X-Ray Reflectivity in Heteroepitaxy: Ho/W(110) *Phys. Rev. Lett.* **79** 3954–7

[203] Yamada C and Kimura T 1995 In-Situ Surface Second-Harmonic Generation Study of Epitaxial Growth of GaAs *Jpn. J. Appl. Phys.* **34** 1102–5

[204] Buhaenko D S, Francis S M, Gouding P A and Pemble M E 1989 Optical second harmonic generation as an in-situ surface diagnostic probe of semiconductor growth processes: I. Adsorption of triethylgallium on GaAs (100) at 300 K *J. Cryst. Growth* **97** 595–8

[205] Jin Q Y, Regensburger H, Vollmer R and Kirschner J 1998 Periodic Oscillations of the Surface Magnetization during the Growth of Co Films on Cu(001) *Phys. Rev. Lett.* **80** 4056–9

[206] Stehlin T, Feller M, Guyot-Sionnest P and Shen Y R 1988 Optical second-harmonic generation as a surface probe for noncentrosymmetric media *Opt. Lett.* **13** 389–91

[207] Vlieg E, van der Gon A W D, van der Veen J F, Macdonald J E and Norris C 1988 Surface X-Ray Scattering during Crystal Growth: Ge on Ge(111) *Phys. Rev. Lett.* **61** 2241–4

[208] Vonk V, Konings S, Barthe L, Gorges B and Graafsma H 2005 Pulsed laser deposition chamber for *in situ* X-ray diffraction *J. Synchrotron Radiat.* **12** 833–4

[209] Dale D, Suzuki Y and Brock J D 2008 In situx-ray reflectivity studies of dynamics and morphology during heteroepitaxial complex oxide thin film growth *J. Phys. Condens. Matter* **20** 264008

[210] Bein B, Hsing H-C, Callori S J, Sinsheimer J, Chinta P V, Headrick R L and Dawber M 2015 In situ X-ray diffraction and the evolution of polarization during the growth of ferroelectric superlattices *Nat. Commun.* **6** 10136

[211] Kowarik S 2016 Thin film growth studies using time-resolved x-ray scattering *J. Phys. Condens. Matter* **29** 43003

[212] Bauer S, Lazarev S, Molinari A, Breitenstein A, Leufke P, Kruk R, Hahn H and Baumbach T 2014

The power of *insitu* pulsed laser deposition synchrotron characterization for the detection of domain formation during growth of $Ba_{0.5}Sr_{0.5}TiO_3$ on MgO *J. Synchrotron Radiat.* **21** 386–94

[213] Liu R, Ulbrandt J G, Hsing H-C, Gura A, Bein B, Sun A, Pan C, Bertino G, Lai A, Cheng K, Doyle E, Evans-Lutterodt K, Headrick R L and Dawber M 2020 Role of ferroelectric polarization during growth of highly strained ferroelectric materials *Nat. Commun.* **11** 2630

[214] Vollmer R, Regensburger H, Wu Y Z and Kirschner J 2001 Magnetization Induced Second Harmonic Generation from Ultrathin Metallic Multilayers *Phys. status solidi* **188** 1513–24

[215] Rubano A, Günter T, Lilienblum M, Aruta C, Miletto Granozio F, Scotti Di Uccio U, Marrucci L, Paparo D and Fiebig M 2015 Optical second harmonic imaging as a diagnostic tool for monitoring epitaxial oxide thin-film growth *Appl. Surf. Sci.* **327** 413–7

[216] Lilienblum M, Lottermoser T, Manz S, Selbach S M, Cano A and Fiebig M 2015 Ferroelectricity in the multiferroic hexagonal manganites *Nat. Phys.* **11** 1070–3

[217] Liu R, Ulbrandt J G, Hsing H-C, Gura A, Bein B, Sun A, Pan C, Bertino G, Lai A, Cheng K, Doyle E, Evans-Lutterodt K, Headrick R L and Dawber M 2020 Role of ferroelectric polarization during growth of highly strained ferroelectric materials *Nat. Commun.* **11** 2630

[218] Fong D D, Kolpak A M, Eastman J A, Streiffer S K, Fuoss P H, Stephenson G B, Thompson C, Kim D M, Choi K J, Eom C B, Grinberg I and Rappe A M 2006 Stabilization of Monodomain Polarization in Ultrathin $PbTiO_3$ Films *Phys. Rev. Lett.* **96** 127601

[219] Stephenson G B and Highland M J 2011 Equilibrium and stability of polarization in ultrathin ferroelectric films with ionic surface compensation *Phys. Rev. B.* **84** 1–15

[220] Efe I, Spaldin N A and Gattinoni C 2021 On the happiness of ferroelectric surfaces and its role in water dissociation: The example of bismuth ferrite *J. Chem. Phys.* **154** 24702

[221] Gattinoni C, Strkalj N, Härdi R, Fiebig M, Trassin M and Spaldin N A 2020 Interface and surface stabilization of the polarization in ferroelectric thin films *Proc. Natl. Acad. Sci.* **117** 28589–95

[222] Mannhart, J and Schlom D G 2010 Oxide Interfaces — An Opportunity for Electronics *Science* **327** 1607–11

[223] Chakhalian J, Millis A J and Rondinelli J 2012 Whither the oxide interface *Nat. Mater.* **11** 92–4

[224] Hwang H Y, Iwasa Y, Kawasaki M, Keimer B, Nagaosa N and Tokura Y 2012 Emergent phenomena at oxide interfaces *Nat. Mater.* **11** 103–13

[225] Chaloupka J and Khaliullin G 2008 Orbital Order and Possible Superconductivity in $LaNiO_3/LaMO_3$ Superlattices *Phys. Rev. Lett.* **100** 16404

[226] Jackeli G and Khaliullin G 2008 Spin, Orbital, and Charge Order at the Interface between Correlated Oxides *Phys. Rev. Lett.* **101** 216804

[227] Koerting V, Yuan Q, Hirschfeld P J, Kopp T and Mannhart J 2005 Interface-mediated pairing in field effect devices *Phys. Rev. B* **71** 104510

[228] Ohtomo A and Hwang H Y 2004 A high-mobility electron gas at the $LaAlO_3/SrTiO_3$ heterointerface *Nature* **427** 423–6

[229] Lee H, Campbell N, Lee J, Asel T J, Paudel T R, Zhou H, Lee J W, Noesges B, Seo J, Park B, Brillson L J, Oh S H, Tsymbal E Y, Rzchowski M S and Eom C B 2018 Direct observation of a two-dimensional hole gas at oxide interfaces *Nat. Mater.* **17** 231–6

[230] Meng M, Wang Z, Fathima A, Ghosh S, Saghayezhian M, Taylor J, Jin R, Zhu Y, Pantelides S T, Zhang J, Plummer E W and Guo H 2019 Interface-induced magnetic polar metal phase in complex oxides *Nat. Commun.* **10** 5248

[231] Cao Y, Wang Z, Park S Y, Yuan Y, Liu X, Nikitin S M, Akamatsu H, Kareev M, Middey S, Meyers D, Thompson P, Ryan P J, Shafer P, N'Diaye A, Arenholz E, Gopalan V, Zhu Y, Rabe K M and Chakhalian J 2018 Artificial two-dimensional polar metal at room temperature *Nat. Commun.* **9** 1547

[232] Mannhart J, Blank D H A and Hwang H Y 2008 Two-Dimensional Fundamentals : Electronic Electron Gases at *Mrs Bull.* **33** 1027–34

[233] Asmara T C, Annadi A, Santoso I, Gogoi P K, Kotlov A, Omer H M, Motapothula M, Breese M B H, Rübhausen M, Venkatesan T, Ariando and Rusydi A 2014 Mechanisms of charge transfer and redistribution in $LaAlO_3/SrTiO_3$ revealed by high-energy optical conductivity *Nat. Commun.* **5**

[234] Willmott P R, Pauli S A, Herger R, Schlepütz C M, Martoccia D, Patterson B D, Delley B, Clarke R, Kumah D, Cionca C and Yacoby Y 2007 Structural Basis for the Conducting Interface between $LaAlO_3$ and $SrTiO_3$ *Phys. Rev. Lett.* **99** 155502

[235] Kalabukhov A S, Boikov Y A, Serenkov I T, Sakharov V I, Popok V N, Gunnarsson R, Börjesson J, Ljustina N, Olsson E, Winkler D and Claeson T 2009 Cationic Disorder and Phase Segregation in $LaAlO_3/SrTiO_3$ Heterointerfaces Evidenced by Medium-Energy Ion Spectroscopy *Phys. Rev. Lett.* **103** 146101

[236] Qiao L, Droubay T C, Kaspar T C, Sushko P V and Chambers S A 2011 Cation mixing, band offsets and electric fields at $LaAlO_3/SrTiO_3$(001) heterojunctions with variable La:Al atom ratio *Surf. Sci.* **605** 1381–7

[237] Yu L and Zunger A 2014 A polarity-induced defect mechanism for conductivity and magnetism at polar-nonpolar oxide interfaces *Nat. Commun.* **5** 1–9

[238] Siemons W, Koster G, Yamamoto H, Harrison W A, Lucovsky G, Geballe T H, Blank D H A and Beasley M R 2007 Origin of Charge Density at $LaAlO_3$ on $SrTiO_3$ Heterointerfaces: Possibility of Intrinsic Doping *Phys. Rev. Lett.* **98** 196802

[239] Savoia A, Paparo D, Perna P, Ristic Z, Salluzzo M, Miletto Granozio F, Scotti Di Uccio U, Richter C, Thiel S, Mannhart J and Marrucci L 2009 Polar catastrophe and electronic reconstructions at the $LaAlO_3/SrTiO_3$ interface: Evidence from optical second harmonic generation *Phys. Rev. B.* **80** 2–7

[240] Rubano A, Fiebig M, Paparo D, Marino A, MacCariello D, Scotti Di Uccio U, Miletto Granozio F, Marrucci L, Richter C, Paetel S and Mannhart J 2011 Spectral and spatial distribution of polarization at the $LaAlO_3/SrTiO_3$ interface *Phys. Rev. B.* **83** 1–6

[241] Rubano A, Günter T, Fink T, Paparo D, Marrucci L, Cancellieri C, Gariglio S, Triscone J M and Fiebig M 2013 Influence of atomic termination on the $LaAlO_3/SrTiO_3$ interfacial polar rearrangement *Phys. Rev. B.* **88** 1–5

[242] Rubano A, Günter T, Fiebig M, Granozio F M, Marrucci L and Paparo D 2018 Ultrafast modification of the polarity at $LaAlO_3/SrTiO_3$ interfaces *Phys. Rev. B* **97** 1–9

[243] Rubano A, Scigaj M, Sánchez F, Herranz G and Paparo D 2019 Optical second harmonic generation from $LaAlO_3/SrTiO_3$ interfaces with different in-plane anisotropies *J. Phys. Condens. Matter* **32** 135001

[244] Grigoriev A, Do D-H, Kim D M, Eom C-B, Adams B, Dufresne E M and Evans P G 2006 Nanosecond Domain Wall Dynamics in Ferroelectric $Pb(Zr,Ti)O_3$ Thin Films *Phys. Rev. Lett.* **96** 187601

[245] Zolotoyabko E, Quintana J P, Hoerman B H and Wessels B W 2002 Fast time-resolved x-ray diffraction in $BaTiO_3$ films subjected to a strong high-frequency electric field *Appl. Phys. Lett.* **80** 3159–61

[246] Grigoriev A, Do D-H, Kim D M K, Eom C-B, Evans P G, Adams B W and Dufresne E M 2006 Nanosecond Structural Visualization of the Reproducibility of Polarization Switching in Ferroelectrics *Integr. Ferroelectr.* **85** 165–73

[247] Grigoriev A, Sichel R J, Jo J Y, Choudhury S, Chen L-Q, Lee H N, Landahl E C, Adams B W, Dufresne E M and Evans P G 2009 Stability of the unswitched polarization state of ultrathin epitaxial $Pb(Zr,Ti)O_3$ in large electric fields *Phys. Rev. B* **80** 14110

[248] Jo J Y, Chen P, Sichel R J, Callori S J, Sinsheimer J, Dufresne E M, Dawber M and Evans P G 2011 Nanosecond Dynamics of Ferroelectric/Dielectric Superlattices *Phys. Rev. Lett.* **107** 55501

[249] Chen P, Cosgriff M P, Zhang Q, Callori S J, Adams B W, Dufresne E M, Dawber M and Evans P G 2013 Field-Dependent Domain Distortion and Interlayer Polarization Distribution in $PbTiO_3/SrTiO_3$ Superlattices *Phys. Rev. Lett.* **110** 47601

[250] Akamatsu H, Yuan Y, Stoica V A, Stone G, Yang T, Hong Z, Lei S, Zhu Y, Haislmaier R C, Freeland J W, Chen L-Q, Wen H and Gopalan V 2018 Light-Activated Gigahertz Ferroelectric Domain Dynamics *Phys. Rev. Lett.* **120** 96101

[251] Chen F, Zhu Y, Liu S, Qi Y, Hwang H Y, Brandt N C, Lu J, Quirin F, Enquist H, Zalden P, Hu T, Goodfellow J, Sher M-J, Hoffmann M C, Zhu D, Lemke H, Glownia J, Chollet M, Damodaran A R, Park J, Cai Z, Jung I W, Highland M J, Walko D A, Freeland J W, Evans P G, Vailionis A, Larsson J, Nelson K A, Rappe A M, Sokolowski-Tinten K, Martin L W, Wen H and Lindenberg A M 2016 Ultrafast terahertz-field-driven ionic response in ferroelectric $BaTiO_3$ *Phys. Rev. B* **94** 180104

[252] Mishina E D, Sherstyuk N E, Stadnichuk V I, Sigov A S, Mukhorotov V M, Golovko Y I, van Etteger A and Rasing T 2003 Nonlinear-optical probing of nanosecond ferroelectric switching *Appl. Phys. Lett.* **83** 2402–4

[253] Lu H A, Wills L A, Wessels B W, Lin W P, Zhang T G, Wong G K, Neumayer D A and Marks T J 1993 Second-harmonic generation of poled $BaTiO_3$ thin films *Appl. Phys. Lett.* **62** 1314–6

[254] Kuo Y-H, Nah S, He K, Hu T and Lindenberg A M 2017 Ultrafast light-induced symmetry changes in single $BaTiO_3$ nanowires *J. Mater. Chem. C* **5** 1522–8

[255] Rubio-Marcos F, Ochoa D A, Del Campo A, García M A, Castro G R, Fernández J F and García J E 2018 Reversible optical control of macroscopic polarization in ferroelectrics *Nat. Photonics* **12** 29–32

[256] Liou Y-D, Chiu Y-Y, Hart R T, Kuo C-Y, Huang Y-L, Wu Y-C, Chopdekar R V, Liu H-J, Tanaka A, Chen C-T, Chang C-F, Tjeng L H, Cao Y, Nagarajan V, Chu Y-H, Chen Y-C and Yang J-C 2019 Deterministic optical control of room temperature multiferroicity in $BiFeO_3$ thin films *Nat. Mater.* **18** 580–7

[257] Stoica V A, Laanait N, Dai C, Hong Z, Yuan Y, Zhang Z, Lei S, McCarter M R, Yadav A, Damodaran A R, Das S, Stone G A, Karapetrova J, Walko D A, Zhang X, Martin L W, Ramesh R, Chen L Q, Wen H, Gopalan V and Freeland J W 2019 Optical creation of a supercrystal with three-dimensional nanoscale periodicity *Nat. Mater.* **18** 377–83

[258] Vats G, Bai Y, Zhang D, Juuti J and Seidel J 2019 Optical Control of Ferroelectric Domains: Nanoscale Insight into Macroscopic Observations *Adv. Opt. Mater.* **7** 1–8

[259] Yang M M and Alexe M 2018 Light-Induced Reversible Control of Ferroelectric Polarization in $BiFeO_3$ *Adv. Mater.* **30** 1–6

[260] Kundys B, Viret M, Colson D and Kundys D O 2010 Light-induced size changes in $BiFeO_3$ crystals *Nat. Mater.* **9** 803–5